Journal of Nepal Geological Society, 2025, Vol. 69, pp. 1-18
https://doi.org/10.3126/jngs.v69i1.88312

Magnetic fabric patterns of tectonic origin in the Triassic carbonates (Tethys Himalaya) of western Dolpo, Nepal

[*]Pitambar Gautam[1] and Erwin Appel[2]

[1]*The Hokkaido University Museum, Hokkaido University, N10W8, Hokkaido 010-0810, Sapporo, Japan*
[2]*Institute of Geosciences, University of Tübingen, Sigwartstrasse 10, Holderlinstrasse 12, 72074 Tübingen, Germany*
[*]*Corresponding author's email: pgautam@museum.hokudai.ac.jp, pitambargautam@yahoo.co.jp*

ABSTRACT

Anisotropy of magnetic susceptibility (AMS) was determined in the impure marly carbonates from 26 sites within the Tethys Himalaya (Tambakurkur (TKF) and Mukut Limestone (MLF) Formations; Triassic age) in upper Dolpo, Western Nepal. Excluding one anomalous site, the average magnetic susceptibility for 25 sites has a range of (76.6±23.7 to 240.3±11.1) $\times 10^{-6}$ SI. Average Jelinek's degree of anisotropy was weak (1.013-1.049), while the AMS ellipsoid shape ranged from moderately prolate to weakly oblate. Ferro(i)magnetic minerals (magnetite with its maghemitized derivatives and pyrrhotite) contributed to remanence. These together with diamagnetic (e.g., calcite) and paramagnetic (e.g., phyllosilicates) minerals contributed to the AMS. Distribution of Principal AMS axes reveals three distinct magnetic fabric patterns (MFPs): (i) A tectonic fabric (MFP1) represented by NE-SW directed magnetic lineations (k_{max} axes) with shallow plunges dominantly to SW (before) or NE (after) bedding tilt-correction) and preferably NW or SE directed shallow plunging k_{min} axes implying a sub-vertical NE-SW magnetic foliation; (ii) A second pattern (MFP2), also of tectonic origin, in which the k_{max} axes exhibit shallow plunge mainly towards N or S and the k_{min} form girdles along an E-W plane (in situ) but align mainly towards E or W after bedding-tilt correction; (iii) a third pattern (MFP3), with the k_{max} axes orthogonal to bedding (S0) that is subparallel to the girdle defined by the other two axes (k_{int} and k_{min}) representing an inverse structural magnetic fabric. MFP1 was clearly acquired before folding, while MFP2 developed during a longer period of active/progressive folding. MFP1 with the mean trend of k_{max} at N46°E (after fold plunge and bedding correction) is interpreted as the reflection of mineral stretching lineation (known from rocks of relatively high grade metamorphics in adjoining areas) formed simultaneously and/or prior to the earliest Eo-Himalayan (D1 and/or D2) deformation events. MFP2, with the mean corrected trend of k_{max} axes at N4°W, is inferred to post-date the MFP1 and correspond to Neo-Himalayan deformation events which promoted thermo-chemical transformations leading to the production of pyrrhotite. Thus, while MFP1 and MFP2 are directly related to the tectonic history of the Higher Himalaya, MFP3 is an inverse structural magnetic fabric, likely controlled by uni-axial/elongated single-domain magnetite grains.

Keywords: Anisotropy of magnetic susceptibility; Magnetic fabric; Magnetite; Tethys Himalaya; Pyrrhotite; Carbonates; Triassic

Received: 4 May 2025 **Accepted:** 3 September 2025

INTRODUCTION

Magnetic susceptibility (MS or k) is a physical property of a material that indicates its capacity to acquire magnetization (M) under an applied magnetic field (H) following the relationship $\mathbf{M}_j = k_{ij}\mathbf{H}_j$ (i,j = 1,2,3), where M and H are vector quantities and k is dimensionless. At low applied fields the magnetization is linear, and the susceptibility is field-independent. The lattice alignment of crystals with magnetocrystalline anisotropy and/or shape alignment of ferro(i)magnetic material (i.e., magnetic minerals/grains with ferromagnetic behavior) in a rock contribute to the anisotropy of magnetic susceptibility (AMS). The rock fabric that commonly involves the preferential distribution-orientation of the constituting minerals gives rise to magnetic anisotropy. For an anisotropic rock specimen, k varies with the measurement direction and represents a 3×3 symmetric second-rank tensor that can be transformed into a triaxial susceptibility ellipsoid, defined by three principal susceptibilities ($k_1 > k_2 > k_3$) with corresponding maximum (k_{max}), intermediate (k_{int}) and minimum (k_{min}) directions. Such AMS ellipsoid reflects the magnetic (susceptibility and its anisotropy) and dimensional (shape, size, and preferred orientation) properties of grains integrated over a volume of the rock sample.

This study, conducted as an extension of a paleomagnetic research (Appel et al. 2012; Crouzet et al. 2003), deals with the magnetic fabric of low-metamorphic grade carbonates exposed in western Dolpo, north central Nepal (Fig. 1). These rocks occur within the core of a synclinorium extending from Dolpo to Manang within the Tethys Himalaya (TH), which is the northernmost longitudinal geotectonic zone within the Nepalese sector of the Himalayan arc (Dhital 2015). The Tethys Himalaya is separated from the Higher Himalaya by a series of north dipping normal faults comprising the South Tibetan Detachment (STD) System (Fig. 1).

The magnetic fabric was determined by measuring the anisotropy of magnetic susceptibility (AMS) at the scale of small cylindrical rock specimens (2.54cm x 2.2cm) aiming at its correlation with the rock fabric and better understanding the microscopic to mesoscopic structures associated with tectono-metamorphic and deformation events within the Tethyan domain (Schill et al. 2003; Parsons et al. 2016; Gautam et al. 2024, 2025). This study complements the paleomagnetic study focused on multicomponent remanence (mainly comprising a post-folding pyrrhotite-based secondary remanence and another pre-folding magnetite-based primary remanence) extracted from the same sites (Crouzet et al. 2003).

SAMPLING AND LABORATORY PROCEDURE

The sampled area lies within the Dolpo-Mugu folded area mapped geologically by Fuchs (1977a). Figure 1c shows the sampling sites within the Triassic Mukut Limestone (MLF) and Tambakurkur Formation (TKF) around and north of Shey Gompa. The MLF (Anisian–Carnian or Aegean to Early Lacian after Garzanti, 1999) is made up of marly limestones and marls, while the TKF (Scythian or Griesbachian after Garzanti, 1999) is made up of pelagic limestones and shales. Through structural analysis of data from Dolpo- Mugu by Fuchs (1973, 1977b) across folds, Stutz (2012) found the folds with axial traces extending for ca. 200 km to possess a half wavelength of 20-50 km and verge south. With the synform in the southwest comprising Mesozoic sedimentary rocks (~9 km minimum thickness: Fuchs 1977b; Colchen et al. 1981) of TH and the core of the antiform in the northeast occupied by the Greater Himalayan Crystallines (GHC) (LeFort, 1976), a structural relief of >9 km (between the crest of antiform to the trough of synform) has been suggested. The dominant structure here is the Dolpo Mang Synclinorium (DMS) with its axis strikes in a NW-SE direction and gently curving. This major structure is accompanied with the secondary folds generally striking parallel to it. Analysis of orientations for fold axes from north to south by Stutz (2012) revealed their shallow but consistent plunge to the SE, and notable shift of synclinorium trend by about 20° (from S64°E in the north to S44°E in the south). Reverse faults, also generally striking NW-SE, occur within the synclinorium. These data together with the involvement of the GHC rocks in folding indicate the deformation to be deep-seated in the Himalayan orogenic wedge. Stutz (2012) assumed the boundary separating the Dhaulagiri limestone at the base of TH from the metamorphic carbonates structurally beneath (intruded by Mugu leucogranites dated at ca. 20.76 Ma to ca. 17.6 Ma by Hurtado et al. (2007) and regarded as the correlatives of the Manaslu leucogranites north of the Annapurna range) to correspond to STD citing the metamorphic and other criteria (Schneider and Masch 1993; Searle and Godin 2003).

In Dolpo and surrounding area, very low to low-grade metamorphic conditions are estimated through illite and chlorite crystallinity and vitrinite reflectance methods (Garzanti et al. 1994; Crouzet et al. 2007). From TH to STD, metamorphic grade generally increases downward and a change from low-temperature deformation mechanisms (e.g., pressure solution affecting fossil shell valves as well as detrital grains) to crystalline plasticity both in quartz and calcite, accompanied by the development of pervasive foliation, occurs in the same

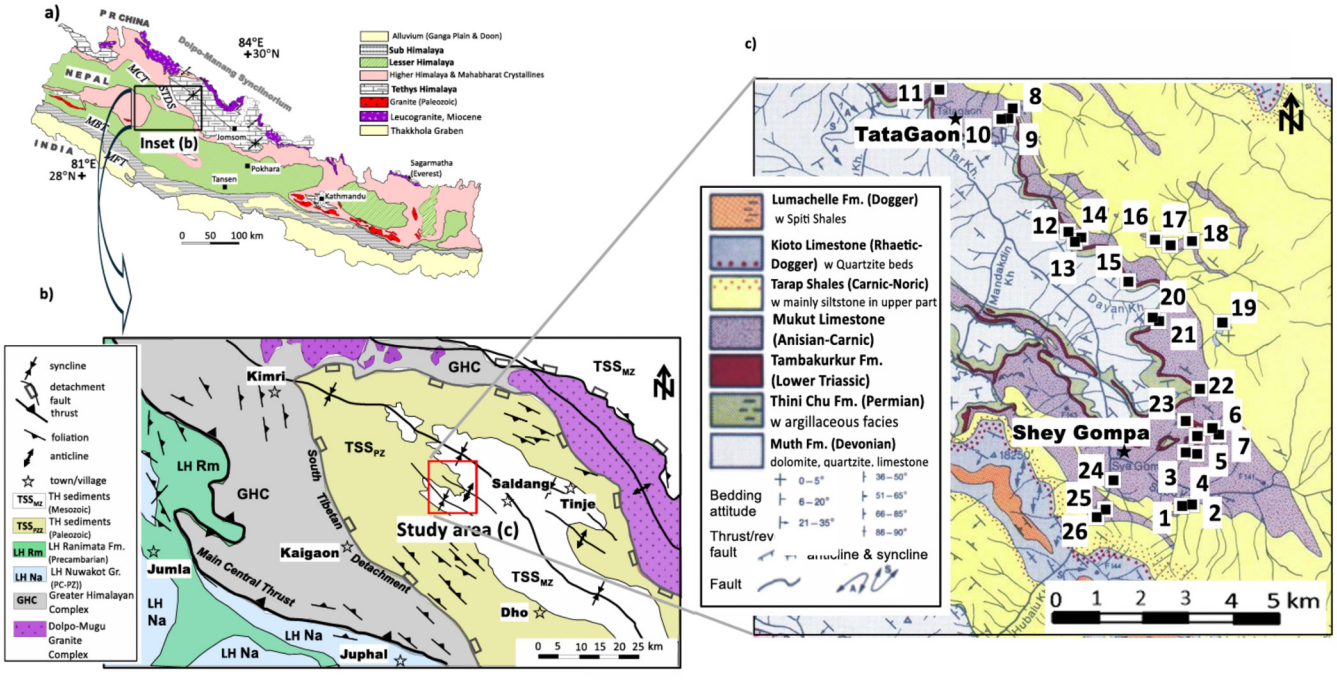

Fig. 1: a) Schematic geologic map of Nepal (adapted after Dhital 2015) showing the major geological units and structural discontinuities (MFT = Main Frontal Thrust, MBT = Main Boundary Thrust, MCT = Main Central Thrust, STDS = Southern Tibet Detachment System), b) regional geological units and structural elements surrounding the study area (Center) in western Dolpo, following Cannon and Murphy (2014), c) locations of sampling sites (for clarity, without pt and pm (indicative of affinity to Tambakurkur Formation and Mukut Limestone) preceding the site number) placed on the extract from geological map of Fuchs (1977a).

direction (Carosi et al. 2007). Information on site locations, sampled lithologies and the geologic units (with formations) etc. related to the carbonate rock specimens are provided in Tables 1 and 2. Additional geotectonic and sampling details appear in Crouzet et al. (2003) that described the characteristic remanent magnetizations of Triassic age (primary, magnetite-based) and Tertiary age (secondary, pyrrhotite-based) from these rocks.

Stutz (2012) suggested that smaller scale folds of the Tethys Himalayan zone within the DMS were formed prior to the STD activation and main folding. STD activation caused the limbs of the fold to go differential rotation that varied with the position along the STD fold. Thus, folds lying structurally above steeper STD folding were rotated more, while those closer to the center of the synclinorium below which the STD folding is less pronounced were rotated less. The synclines formed prior to STD folding with presumably horizontal plunges were locally rotated after STD folding to develop gently dipping plunges, especially at the nose of synclinorium. The axis of the synclinorium itself is gently curvilinear with strikes in a NW-SE direction. For the area sampled in this study, the fold axis following the folding of the STD is estimated to be directed towards S54°E with a plunge of 12°, which is used during the first step of correction of the directions of AMS axes and the bedding poles – used subsequently for the second step of bedding-tilt correction. Several studies (Searle and Godin 2003; Godin et al. 2006; Gleeson and Godin 2005) hint to the cessation of the STD by ca. 19-16 Ma. Such inference implies that Dolpo-Mugu fold structures were developed during or after the early Miocene. Folding might have continued till ca. 11 Ma that corresponds to the timing of the extensional faulting found to crosscut the folds in the Thakkola graben (Garzione et al. 2003).

The Dolpo-Mugu folds may be related to similar large-scale folds situated at either sides along the E-W direction (Stutz 2012). In the Manaslu region of central Nepal, east of the Thakkhola graben and approximately 200 km from the Dolpo- Mugu folds, there is a pair of large-scale folds called the Chako antiform and Mutsog synform. Like the Dolpo- Mugu folds these folds developed after slip on the STD ceased and have GHC in the core of the antiform and TH in the core of the synform. The hinge of the Mustog synform plunges 10° towards the NW. The Chako antiform plunges 8° to the NW. The folds are upright, open folds with amplitude of ~4 km and a wavelength of ~25 km (Gleeson and Godin, 2006). The large magnitude of these folds, like the Dolpo-Mugu folds, is considered as indicative of the crustal-scale folding.

Table 1: Field sampling details with magnetic susceptibility and natural remanent magnetization (NRM) data at site level

		GPS coordinates				*Bedding (S0)*		Magnetic susceptibility							NRM	
		Latitude	Longitude	Altitude	No. of	Dip dir	Dip amount	Average	stdev	Min	First quartile	Median	hird quartile	Max	J_{NRM}	stdev
S. No.	Site	(deg. N)	(deg. E)	(m)	cores*	(deg.)		(10^{-6} SI)							(mAm^{-1})	
Geological unit: Mukut Limestone; Lithology: marly limestones and marls; Age: Triassic (Anisian–Carnian or Aegean to Early Lacian)																
1	pm1	29.3420	82.9798	4380	10	172	16	160.1	44.2	143.0	143.0	147.0	150.0	259.0	5.04	5.17
2	pm2	29.3420	82.9798	4410	11	226	28	137.9	58.9	94.3	94.3	113.4	164.8	240.0	3.09	2.05
3	pm6	29.3577	82.9833	4680	10	128-218	15-70	530.4	93.1	454.5	454.5	512.5	594.5	691.0	1.12	1.06
4	pm7	29.3577	82.9833	4690	10	110	15	171.6	78.9	103.8	103.8	144.0	231.3	309.0	0.41	0.17
5	pm8	29.4247	82.9410	4200	8	40	35 (85/sp 8)	135.7	35.4	130.5	130.5	134.0	155.5	175.0	0.92	0.26
6	pm9	29.4243	82.9403	4220	10	40	55	170.4	88.8	126.0	126.0	160.0	215.0	359.0	1.16	0.43
7	pm10	29.4231	82.9383	4140	10	351	32	164.4	26.2	142.8	142.8	162.0	189.9	194.8	0.82	0.35
8	pm11	29.4302	82.9212	4090	10	225-245	33-40	205.8	32.3	181.3	181.3	218.0	230.8	235.0	0.97	0.45
9	pm14	29.3979	82.9547	4705	10	45	26	163.6	36.4	135.0	135.0	156.0	174.0	222.0	2.00	0.86
11	pm16	29.3973	82.9708	4570	10	18	24	226.4	52.4	189.0	189.0	212.5	241.8	331.0	1.44	0.74
12	pm17	29.3963	82.9743	4525	10	36	28	211.6	33.3	191.0	191.0	211.0	236.0	269.0	1.27	0.41
13	pm18	29.3982	82.9797	4500	10	354	43	158.0	44.7	135.5	135.5	139.5	162.0	258.0	1.05	0.95
14	pm19	29.3806	82.9870	4670	10	24	47	229.1	38.9	193.0	193.0	229.0	235.0	300.0	3.58	1.67
15	pm21	29.3767	82.9732	4720	10	102	13	203.6	41.1	169.0	169.0	190.0	240.0	268.0	1.54	0.57
16	pm23	29.3602	82.9797	4775	10	185	34	240.3	11.1	237.0	237.0	240.0	241.0	257.0	2.38	0.07
17	pm24	29.3472	82.9618	4235	10	6	74	164.8	64.9	128.0	128.0	151.0	177.5	284.0	1.87	2.03
18	pm25	29.3433	82.9657	4360	10	215	50	200.2	46.6	169.0	169.0	191.0	218.5	287.0	1.17	0.29
19	pm26	29.3318	82.9633	4410	10	220	17	182.9	54.3	139.8	139.8	181.5	221.8	255.0	2.89	1.55
Geological unit: Tambakurkur Formation; Lithology: pelagic limestones; Age: Triassic (Scythian or Griesbachian)																
20	pt3	29.3517	82.9787	4410	10	218	42	161.1	36.0	134.0	134.0	158.5	187.5	207.0	0.64	0.22
21	pt4	29.3529	82.9798	4460	11	208	33	92.0	24.6	61.1	61.1	95.5	113.0	156.0	0.51	0.42
22	pt5	29.3561	82.9819	4590	10	160	17	99.1	30.1	77.7	77.7	91.1	127.0	134.0	0.64	0.48
23	pt12	29.3994	82.9512	4615	10	52	22	76.6	23.7	63.8	63.8	78.3	90.3	110.0	0.64	0.71
24	pt13	29.3974	82.9531	4660	10	212	19	178.1	52.5	171.0	171.0	192.0	206.0	241.0	0.40	0.20
10	pt15	29.3904	82.9628	4615	10	50	20	178.9	57.2	190.0	190.0	202.0	209.0	216.0	8.79	11.08
25	pt20	29.3817	82.9727	4585	10	130	22	84.2	25.5	69.9	69.9	89.4	113.8	172.0	0.48	0.53
26	pt22	29.3655	82.9830	4740	10	52	32	137.1	26.8	116.8	116.8	133.0	153.5	170.0	2.55	1.60

* Number of independently drilled and oriented cores. Specimens used in calculation of magnetic susceptibility and NRM may differ.

Isothermal remanent magnetization (IRM) acquisition by specimens from 9 sites involved applying increasingly higher magnetic fields of up to 2.5 T field using a MMPM9 pulse magnetizer (Magnetic Measurements) and subsequently measuring the acquired IRM by a fluxgate spinner magnetometer (Molspin) with a noise level ca. 0.2 mAm^{-1} (for 10-cm^3 samples). A Kappabridge KLY-2 (Agico) was used to measure the AMS of each specimen in 15 different positions (following Jelinek's scheme). Magnetic measurements were carried out at the paleomagnetic laboratory of the University of Tübingen. IRM was analyzed with log-Gaussian decomposition quantified by median acquisition fields (B1/2) and the half-width of the logarithmic dispersion parameter (DP) (Kruiver et al. 2001). Interactive AMS data processing and plotting directions were performed using the Anisoft6 program (Agico) (Chadima 2018).

BACKGROUND INFORMATION ON MS, ITS ANISOTROPY AND MAGNETIC FABRIC

MS of minerals constituting low metamorphic grade sedimentary rocks

The magnitude of bulk MS of a rock is often determined by the relative content of a few ferro(i)magnetic minerals. The magnetic minerals expected in the samples studied are: soft magnetic minerals such as magnetite and maghemite (mass-specific susceptibility in the order of 10^{-3} m^3kg^{-1}), and hard magnetic minerals such as pyrrhotite (mostly about two orders lower), hematite and goethite (mostly about three to four orders lower) arranged in the order of increasing hardness (Hunt et al. 1995; Dearing 1999; Peters and Dekkers 2003; Lascu et al. 2010). For superparamagnetic grains, i.e., single domain (SD) particles <25 nm in size for magnetite (but different thresholds dependent upon relaxation times for others) in which the acquired magnetic remanence vanishes instantaneously, the susceptibility values are expected to be one order of magnitude higher (Dunlop and Özdemir 1997). The bulk susceptibility of carbonates, often impure, is predominated by the contributions from diamagnetic (calcite: -8×10^{-9} m^3kg^{-1}, water and organic matter: -9.0×10^{-9} m^3kg^{-1}, quartz: -6.0×10^{-9} m^3kg^{-1}), paramagnetic (feldspar), and imperfect antiferromagnetic minerals including hematite (Rochette 1987; Dearing 1999; Lascu et al. 2010).

Basic AMS parameters

In this study, the magnetic fabric in a rock sample is characterized by (i) three principal AMS magnitudes and directions (maximum kmax ≥ intermediate kint ≥ minimum kmin), (ii) shape parameter (T), and (iii) corrected degree of anisotropy (PJ). T and PJ are calculated as follows (Jelinek 1981):

$$T = \left(2\eta_{\text{int}} - \eta_{\max} - \eta_{\min}\right) / \left(\eta_{\max} - \eta_{\min}\right)$$

$$P_j = \exp\sqrt{2\left[\left(\eta_{\max} - \eta_m\right)^2 + \left(\eta_{\text{int}} - \eta_m\right)^2 + \left(\eta_{\min} - \eta_m\right)^2\right]}$$

where, ηmax = ln kmax; ηint = ln kint; ηmin = ln kmin; ηm = ln km, and km = (kmax + kint + kmin)/3 is the mean MS.

For samples with negative bulk MS, due to the dominant contribution of diamagnetic minerals, the principal AMS parameters were determined considering the negative sign following Hrouda (2004). This approach ensures correctly calculating the majority of the scalar parameters except for T, which requires the use of the following expression:

$$T = 2(\eta\text{int} - \eta\text{min})/(\eta\text{max} - \eta\text{min})-1$$

Several other AMS factors, whose definitions are briefly given in the footnote in Table 2, commonly used while comparing with parameters for petrofabric analysis, were also calculated.

MAGNETOMINERALOGY

IRM analysis

Indirect inferences on magnetic minerals were made by IRM acquisition (in fields up to 2.5 T), and subsequent IRM unmixing (Kruiver et al. 2001). Figure 2 illustrates IRM acquisition and demagnetization response with representative data from Gaussian decomposition of the IRM gradient. Three components, namely Comp1 with low (~30-40 mT), Comp2 with intermediate (~55-70 mT) and Comp3 with high (~190-300 mT) ranges of B1/2 were recognized. Concerning DP, Comp1 had a distinctly high value (0.35) than others characterized by values within a narrower range (0.15-0.25). Comp1 and Comp3 are interpreted to represent magnetite and pyrrhotite (Peters and Dekkers 2003), which carry of the characteristic primary and secondary and paleo- remanences (Crouzet et al. 2003). Comp2 is likely to represent strongly maghemitized magnetite, produced by inhomogeneous low-temperature oxidation that causes particle-internal heterogeneity and, as a result, fining of the domain state and increasing magnetic hardness due to heterogeneous stress distribution (Zhang et al. 2020).

Thermal variation of MS

Subsamples of carbonates from Dolpo exhibit paramagnetic behavior upon heating as shown by a hyperbolic decay of MS upon heating up to about 450°C (specimen pm26-2, Fig. 3). The susceptibility starts to increase at varying degree yielding a peak around 525-530°C followed by rapid decay to almost zero already by around 600°C (specimens pm26-2 and pm1-2b). The susceptibility enhancement is attributed to neo-formation of magnetite during heating at >400-450°C. The level of MS clearly above zero before the increase in connection with complete susceptibility decay near 580°C indicates that the sample also contains original magnetite. It is possible to discern pyrrhotite (see the shaded zones A in specimen pm1-2b) from the Curie temperature of about 325°C) (Fig. 3). Magnetite is recognized with a greater certainty by the point of initiation of the linear segment (paramagnetic behavior; Petrovský and Kapička 2006) in the inverse susceptibility curve at ca. 580°C.

These magneto-mineralogical data together with the alternating field and thermal demagnetization behavior of the carbonates in Dolpo suggest the presence of magnetite, maghemite and pyrrhotite. Various origins (detrital, authigenic) of magnetite and maghemite in the pelagic marine carbonates is discussed by Roberts et al. (2013), whereas the low metamorphic grade origin of pyrrhotite during the Tertiary by various secondary processes (conversion from magnetite, reduction from pyrite, etc.) is discussed in Appel et al. (2012).

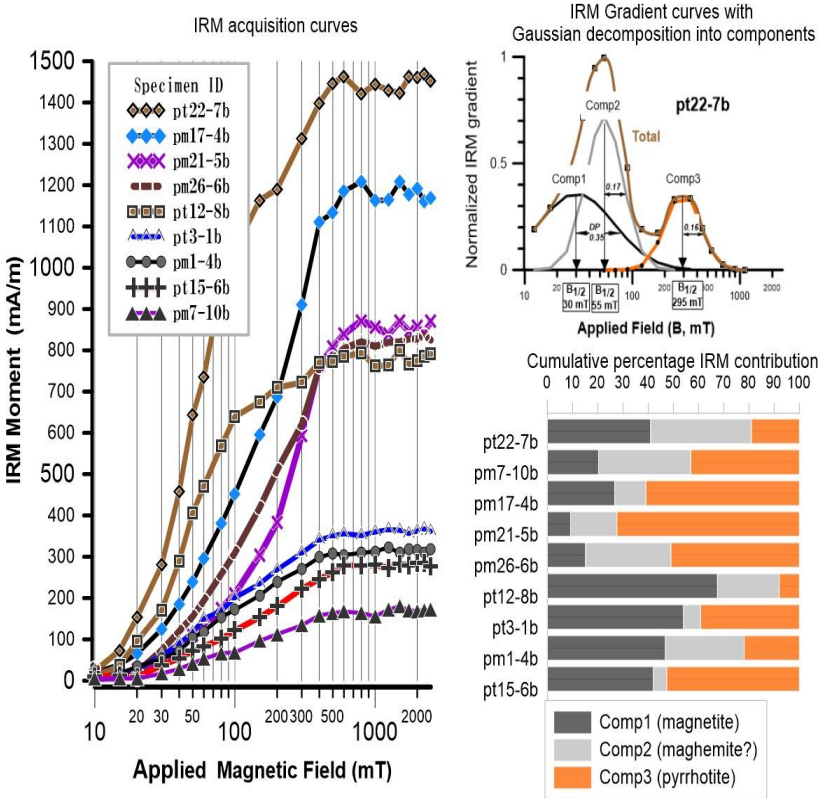

Fig 2: Results of IRM acquisition and analysis for magnetic minerals. Left: IRM acquisition curves (up to 2.5 T) for specimens from 9 sites. Right, above: Results of Gaussian decomposition of the IRM gradient into three components for a representative specimen. Each IRM gradient curve can be reasonably modelled by Gaussian curves for three components (Comp1-3) described by median acquisition field (B1/2) and logarithmic dispersion parameter (DP). Right, below: Relative percentage IRM contribution of components (inferred minerals) in each specimen. The three components with increasing B1/2 are inferred to represent magnetite, maghemitized derivative of magnetite and pyrrhotite.

RESULTS

Bulk MS and NRM data

Results of AMS measurements, NRM data and basic information at the level of specimen and site in various modes are presented in Tables 1-3. Among the MLF sites, 17 sites exhibit average MS of (135.6±35.4 to 240.3±11.1)×10^{-6} SI), whereas a much higher value (530.4±93.1)×10^{-6} SI characterizes the anomalous site pm6. Eight sites from the TKF yield slightly lower range: (76.6±23.7-178.9±52.7)×10^{-6} SI. Considering a skewed (commonly lognormal) distribution of km, horizontal boxplots with site level quartiles for each formation (with sites arranged in the order of the natural remanent magnetization (NRM) intensity (J_{NRM})), and susceptibility versus J_{NRM} biplots (Fig. 4). For MLF sites, the interquartile range (IQR, shown by the width of each box in Fig. 4) for 17 sites is 95-270×10^{-6} SI, while the site pm6 has distinctly higher range (460-610)×10^{-6} SI. The TKF sites yield a slightly lower IQR of (60-210)×10^{-6} SI. These values suggest that the bulk susceptibility in sites other than pm6 is controlled by paramagnetic and diamagnetic minerals, with small difference between formations. The biplot reveals elevated J_{NRM} at two sites (pm1 and pt15), but no straightforward relationship between MS and J_{NRM} exists. It is expected that different sets of minerals, with varying grain size ranges, exert control on the susceptibility (mainly paramagnetic contribution) and NRM (ferro(i)magnetic contribution) magnitudes although even a small amount of ferro(i)magnetic minerals such as magnetite may have dominant control on AMS in the weakly magnetic lithofacies.

Magnetic fabric characteristics based on the scalar AMS parameters

Relationships between AMS scalar parameters (K_m and T versus P_J) at site level are shown concisely in Fig. 5. Specimen level data were partly illustrated in Fig. 4 and their details presented in Table 2. Site pm6 in MLF, unique for its location at the closure of a fold and display of a large variation of bedding attitudes at core-drilling location and with distinct mean MS (Figs. 4, and 5), exhibits elevated magnitudes of T (0.754) and P_J (1.116) indicative of highly oblate AMS ellipsoid and relatively well-developed degree of anisotropy (Fig. 5). In contrast, the ranges of P_J for 17 MLF sites and 8 TKF sites are rather low at 1.015-1.049 and 1.013-1.035, respectively. In general, the MLF specimens are more anisotropic than the TKF specimens. The ranges of shape parameter are not so distinct (MLF: -0.439 to 0.147; TKF: -0.254 to 0.285), and many sites show affinity to triaxial AMS ellipsoids. The percent anisotropy (h%; Tauxe et al. 1990) clearly distinguishes site pm6 (average: 3.33%; a range: 2.3-4.8%) from the other sites (average: 0.89%, range: 0.07-2.6%) based on aggregation of data presented in Table 2. The distinctly high values for the pm6 specimens may be explained by the relatively higher

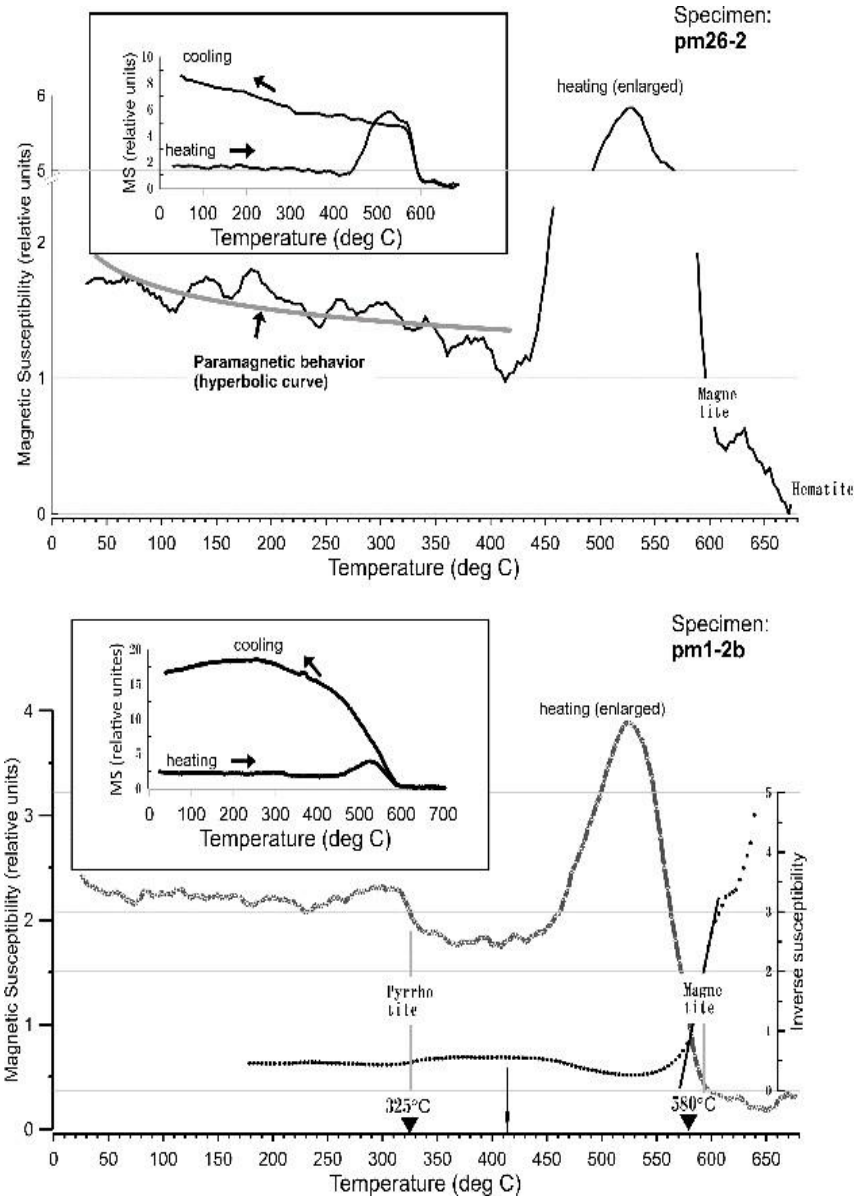

Fig 3: Curves showing the thermal variation of low-field magnetic susceptibility of subsamples (chips) of two specimens from Sites pm1 (below) and pm26 (above). The insets in each curve shows the complete heating-cooling cycles in air. The heating curves are used to infer the magnetic minerals (pyrrhotite and magnetite, original and newly produced; hematite, most likely newly produced) based on characteristic points such as Curie temperature and paramagnetic behavior above such points.

degree of deformation associated with regional metamorphism and locally enhanced heat-induced mineral transformations. Except for that site, both formations exhibit low magnitudes of the scalar AMS parameters, with the MLF sediments being slightly stronger in average than those from the TKF sites (Tables 2, and 3).

Magnetic fabric patterns based on the principal AMS directions

AMS scalar parameters at specimen level in Table 2 are provided with the specimen level test statistics for the judgement of development of lineation (e12), foliation (e23), and the mathematical equivalent of F-test statistic (e31), which are computed during the calculation of the AMS tensor (Jelinek 1977). Each specimen is assigned the "dominant element" according to the threshold for lineation (e12 <=25°), foliation (e23 <=25°), and none (commonly, e31 <=20°, above which the specimen is considered to behave as isotropic; but even for a smaller value when both e12 and e23 exceed the threshold of 25°). Directional analysis of the AMS axes hereafter excludes the isotropic specimens labelled as 'none' in Table 2. For the sake of completeness of data, Table 3 lists the principal AMS directions (k_{max} and k_{min}, with Jelinek's confidence ellipse parameters) at the site level calculated using all data in Table 2. To highlight the significant intra-site as well as specimen level variations at each site, the directional plots in stereonet show

values at specimen level (Figs. 6 and 8).

Table 2: Scalar parameters related to magnetic fabric based on anisotropy of magnetic susceptibility (AMS) at specimen level

S. No.	Specimen	Field ency		(in SI)	L	F	P	P_J	T	U	Q	E	h%	e12	e23	e31	element
Mukut Limestone																	
1	pm1-2b	423	875	1.40E-04	1.037	1.005	1.043	1.047	-0.756	-0.760	1.572	0.969	1.398	3.1	21.4	2.7	lineation
2	pm1-3	423	875	2.59E-04	1.011	1.010	1.022	1.022	-0.051	-0.056	0.718	0.999	0.712	6.2	6.9	3.3	lineation
3	pm1-6	423	875	1.52E-04	1.027	1.001	1.027	1.031	-0.950	-0.951	1.904	0.975	0.898	3.9	69.7*	3.8	lineation
4	pm1-7	423	875	1.47E-04	1.019	1.018	1.038	1.038	-0.028	-0.038	0.701	0.999	1.24	28.3*	30.1*	15.6	none
5	pm1-8b	423	875	1.46E-04	1.032	1.006	1.038	1.041	-0.706	-0.711	1.495	0.974	1.252	3	17.2	2.6	lineation
6	pm1-9b	423	875	1.48E-04	1.016	1.009	1.026	1.026	-0.273	-0.279	0.940	0.993	0.853	6.9	12	4.4	lineation
7	pm1-10	423	875	1.29E-04	1.011	1.008	1.019	1.019	-0.142	-0.146	0.803	0.997	0.615	16	21	9.3	lineation
8	pm2-2	423	875	9.46E-05	1.015	1.011	1.026	1.026	-0.154	-0.160	0.817	0.996	0.846	8.7	11.9	5.1	lineation
9	Pm2-4	423	875	2.40E-04	1.019	1.034	1.053	1.054	0.293	0.281	0.438	1.015	1.723	25.2	14.8	9.6	foliation
10	Pm2-5b	423	875	9.57E-05	1.012	1.008	1.020	1.020	-0.195	-0.200	0.857	0.996	0.644	17.9	25.8*	11	lineation
11	Pm2-6b	423	875	8.75E-05	1.030	1.006	1.037	1.039	-0.650	-0.655	1.412	0.977	1.209	7.4	32.1*	6.2	lineation
12	Pm2-7b	423	875	1.31E-04	1.009	1.006	1.014	1.015	-0.203	-0.206	0.863	0.997	0.477	11.1	16.6	6.7	lineation
13	Pm2-8b	423	875	9.33E-05	1.025	1.011	1.036	1.037	-0.411	-0.418	1.099	0.986	1.188	5.6	13.4	4	lineation
14	Pm2-10b	423	875	1.49E-04	1.022	1.004	1.026	1.028	-0.703	-0.706	1.487	0.983	0.842	6.6	33.8*	5.6	lineation
15	Pm2-11b	423	875	2.12E-04	1.012	1.008	1.020	1.020	-0.195	-0.199	0.856	0.996	0.661	15.2	22.1	9.2	lineation
16	pm6-1b	423	875	6.08E-04	1.012	1.084	1.096	1.105	0.748	0.738	0.140	1.071	3.022	17.5	2.7	2.4	foliation
17	pm6-4b	423	875	4.84E-04	1.014	1.082	1.096	1.104	0.707	0.696	0.165	1.067	3.03	3.8	0.7	0.6	foliation
18	pm6-5c	423	875	6.91E-04	1.006	1.065	1.072	1.080	0.828	0.822	0.093	1.059	2.289	15.9	1.6	1.5	foliation
19	pm6-6b	423	875	4.59E-04	1.012	1.079	1.092	1.100	0.729	0.718	0.152	1.066	2.889	9.6	1.6	1.4	foliation
20	pm6-7b	423	875	5.41E-04	1.013	1.080	1.094	1.102	0.709	0.697	0.164	1.066	2.968	11.3	2	1.7	foliation
21	pm6-8b	423	875	5.90E-04	1.008	1.095	1.104	1.116	0.845	0.838	0.085	1.087	3.245	20.8	1.9	1.8	foliation
22	pm6-9b	423	875	4.41E-04	1.017	1.120	1.139	1.152	0.746	0.732	0.144	1.102	4.265	15.7	2.5	2.2	foliation
23	pm6-10	423	875	4.30E-04	1.021	1.133	1.157	1.171	0.717	0.699	0.163	1.110	4.763	11.4	2.1	1.7	foliation
24	pm7-3b	423	875	1.03E-04	1.009	1.003	1.012	1.012	-0.516	-0.518	1.224	0.994	0.391	11.7	33.1*	8.9	lineation
25	pm7-4b	423	875	3.09E-04	1.005	1.003	1.008	1.008	-0.131	-0.133	0.790	0.999	0.262	22.2	28.1*	13	lineation
26	pm7-5b	423	875	9.98E-05	1.007	1.008	1.015	1.015	0.097	0.094	0.586	1.001	0.486	22.8	19.2	10.8	foliation
27	pm7-6b	423	875	1.62E-04	1.006	1.004	1.010	1.010	-0.261	-0.264	0.924	0.997	0.338	16.5	27*	10.6	lineation
28	pm7-7	423	875	1.26E-04	1.009	1.007	1.016	1.016	-0.090	-0.094	0.753	0.999	0.539	8.5	10.2	4.7	lineation
29	pm7-8	423	875	2.41E-04	1.009	1.006	1.016	1.016	-0.200	-0.204	0.861	0.997	0.516	10.8	16.1	6.5	lineation
30	pm7-9	423	875	2.28E-04	1.018	1.008	1.026	1.026	-0.360	-0.366	1.037	0.991	0.85	7.3	15.4	5	lineation
31	pm7-10	423	875	1.04E-04	1.012	1.001	1.013	1.014	-0.837	-0.838	1.701	0.990	0.421	15.6	72.5*	14.4	lineation
32	pm8-1b	423	875	1.28E-04	1.012	1.012	1.024	1.024	0.001	-0.005	0.671	1.000	0.797	26*	26.3*	13.8	none
33	pm8-2b	423	875	1.34E-04	1.030	1.010	1.040	1.042	-0.477	-0.485	1.181	0.981	1.324	3.2	9.1	2.4	lineation
34	pm8-3b	423	875	1.38E-04	1.017	1.023	1.040	1.040	0.168	0.158	0.533	1.007	1.306	5.6	4.1	2.4	lineation
35	pm8-4b	423	875	1.33E-04	1.006	1.014	1.020	1.021	0.397	0.392	0.358	1.008	0.672	19.4	8.8	6.1	foliation
36	pm8-6	423	875	1.75E-04	1.028	1.023	1.051	1.051	-0.106	-0.118	0.776	0.995	1.659	4.9	6.2	2.7	foliation
37	pm8-7	423	875	1.73E-04	1.007	1.017	1.023	1.024	0.438	0.433	0.330	1.010	0.763	15	6.1	4.3	foliation
38	pm8-8b	423	875	6.86E-05	1.008	1.016	1.024	1.025	0.301	0.295	0.428	1.007	0.799	38.6*	23.5	15.7	foliation
39	pm9-1	423	875	6.01E-05	1.024	1.035	1.060	1.060	0.176	0.162	0.530	1.010	1.926	8.8	6.4	3.7	foliation
40	pm9-2	423	875	7.78E-05	1.019	1.024	1.044	1.044	0.107	0.097	0.583	1.005	1.428	10.2	8.4	4.6	foliation
41	pm9-4	423	875	1.49E-04	1.020	1.009	1.029	1.030	-0.410	-0.416	1.095	0.988	0.958	15.5	33.9*	11.1	lineation
42	pm9-5	423	875	1.60E-04	1.016	1.016	1.032	1.032	0.004	-0.004	0.670	1.000	1.05	5.6	5.7	2.8	lineation
43	pm9-6	423	875	1.26E-04	1.015	1.023	1.038	1.038	0.221	0.213	0.490	1.008	1.225	17.5	11.6	7.1	foliation
44	pm9-7	423	875	1.69E-04	1.022	1.015	1.037	1.037	-0.194	-0.203	0.860	0.993	1.209	4.8	7.2	2.9	lineation
45	pm9-8	423	875	3.59E-04	1.020	1.004	1.024	1.026	-0.633	-0.637	1.385	0.985	0.799	3.7	16.4	3.1	lineation
46	pm9-9	423	875	2.17E-04	1.039	1.010	1.050	1.052	-0.591	-0.599	1.332	0.972	1.618	4.6	17.8	3.7	lineation
47	pm9-10	423	875	2.15E-04	1.023	1.007	1.031	1.032	-0.521	-0.527	1.235	0.984	1.017	7.9	24.2	6.1	lineation
48	pm10-1	423	875	1.95E-04	1.024	1.012	1.036	1.036	-0.322	-0.330	0.996	0.989	1.171	8.6	16.7	5.7	lineation
49	pm10-2	423	875	1.41E-04	1.013	1.035	1.049	1.051	0.448	0.438	0.327	1.022	1.582	18.4	7.4	5.3	foliation
50	pm10-3	423	875	1.76E-04	1.024	1.005	1.028	1.030	-0.675	-0.679	1.447	0.981	0.927	6.6	31.2*	5.6	lineation
51	pm10-4	423	875	1.48E-04	1.008	1.014	1.022	1.022	0.295	0.290	0.432	1.006	0.715	13.5	7.5	4.9	foliation
52	pm10-5	423	875	1.89E-04	1.005	1.027	1.032	1.034	0.684	0.680	0.174	1.022	1.04	14.2	2.8	2.3	foliation
53	pm10-6	423	875	1.92E-04	1.010	1.018	1.028	1.028	0.271	0.265	0.451	1.007	0.906	13.3	7.8	5	foliation
54	pm10-9	423	875	1.31E-04	1.005	1.016	1.021	1.022	0.511	0.508	0.281	1.011	0.678	32.8*	11.9	9	foliation
55	pm10-10	423	875	1.44E-04	1.020	1.018	1.039	1.039	-0.033	-0.043	0.705	0.999	1.259	6.1	6.7	3.2	foliation
56	pm11-1	423	875	2.09E-04	1.041	1.008	1.049	1.053	-0.683	-0.689	1.462	0.968	1.597	3.6	19.1	3.1	lineation
57	pm11-3	423	875	1.72E-04	1.037	1.023	1.061	1.062	-0.241	-0.255	0.914	0.986	1.975	6.6	11.1	4.2	lineation
58	pm11-4	423	875	2.35E-04	1.005	1.025	1.031	1.033	0.642	0.638	0.199	1.020	0.998	30.1*	7.3	6	foliation
59	pm11-7	423	875	2.32E-04	1.019	1.011	1.030	1.030	-0.273	-0.279	0.940	0.992	0.974	6.9	12.2	4.5	lineation
60	pm11-8	423	875	2.27E-04	1.015	1.005	1.020	1.021	-0.501	-0.505	1.206	0.990	0.658	8	23.1	6	lineation
61	pm11-9	423	875	1.61E-04	1.012	1.009	1.020	1.020	-0.144	-0.149	0.806	0.997	0.67	10.9	14.5	6.3	lineation
62	pm14-1	423	875	1.74E-04	1.018	1.006	1.023	1.024	-0.505	-0.509	1.212	0.988	0.772	7.2	21.3	5.5	lineation
63	pm14-2	423	875	1.56E-04	1.022	1.006	1.028	1.029	-0.548	-0.553	1.269	0.985	0.926	6.2	20.7	4.8	lineation
64	pm14-4	423	875	2.22E-04	1.007	1.011	1.019	1.019	0.225	0.221	0.484	1.004	0.614	18.7	12.2	7.5	foliation
65	pm14-5	423	875	2.18E-04	1.007	1.018	1.025	1.026	0.464	0.459	0.313	1.012	0.818	17.3	6.6	4.8	foliation
66	pm14-6	423	875	1.24E-04	1.009	1.008	1.017	1.017	-0.096	-0.101	0.759	0.998	0.562	28.6*	33.7*	16.7	none

continued to next page

S. No.	Specimen	Field	Frequ-ency	Kmean (in SI)	L	F	P	P_J	T	U	Q	E	h%	e12	e23	e31	Dominant element
67	pm14-7	423	875	1.35E-04	1.024	1.005	1.029	1.031	-0.635	-0.640	1.389	0.982	0.949	6	25.6*	4.9	lineation
68	pm14-8	423	875	1.25E-04	1.022	1.017	1.039	1.039	-0.133	-0.142	0.799	0.995	1.27	6.9	9.1	3.9	lineation
69	pm14-9	423	875	1.66E-04	1.019	1.007	1.027	1.028	-0.439	-0.444	1.130	0.989	0.883	8.5	21.3	6.2	lineation
70	pm14-9	423	875	1.53E-04	1.028	1.011	1.040	1.041	-0.433	-0.441	1.126	0.983	1.301	8.5	21.3	6.2	lineation
71	pm16-1b	423	875	2.00E-04	1.023	1.017	1.041	1.041	-0.153	-0.163	0.820	0.994	1.334	3.1	4.4	1.8	lineation
72	pm16-2	423	875	2.71E-04	1.015	1.009	1.024	1.024	-0.240	-0.246	0.904	0.994	0.785	7.3	11.9	4.5	lineation
73	pm16-4	423	875	3.31E-04	1.027	1.013	1.041	1.041	-0.332	-0.341	1.008	0.987	1.329	3.5	7	2.3	lineation
74	pm16-5	423	875	2.32E-04	1.017	1.020	1.038	1.038	0.071	0.061	0.613	1.003	1.233	8.9	7.9	4.2	foliation
75	pm16-6	423	875	1.89E-04	1.017	1.004	1.021	1.022	-0.607	-0.610	1.347	0.987	0.697	5.6	22.1	4.5	lineation
76	pm16-7	423	875	1.89E-04	1.023	1.007	1.030	1.032	-0.535	-0.540	1.252	0.984	0.998	4	13.2	3.1	lineation
77	pm16-9	423	875	2.25E-04	1.022	1.008	1.030	1.031	-0.476	-0.481	1.176	0.986	0.988	6.7	18.4	4.9	lineation
78	pm16-10	423	875	1.75E-04	1.012	1.018	1.030	1.031	0.200	0.193	0.506	1.006	0.997	10.1	6.8	4.1	foliation
79	pm17-1	423	875	1.66E-04	1.025	1.025	1.051	1.051	0.003	-0.010	0.675	1.000	1.648	5.3	5.4	2.7	lineation
80	pm17-2	423	875	1.91E-04	1.018	1.025	1.043	1.043	0.160	0.150	0.540	1.007	1.386	5.1	3.8	2.2	foliation
81	pm17-3	423	875	2.11E-04	1.036	1.009	1.045	1.048	-0.609	-0.616	1.355	0.973	1.483	2.3	9.5	1.8	lineation
82	pm17-5	423	875	1.97E-04	1.042	1.004	1.046	1.051	-0.837	-0.841	1.705	0.963	1.508	4.5	42.4*	4.2	lineation
83	pm17-6	423	875	2.69E-04	1.008	1.017	1.025	1.025	0.377	0.371	0.373	1.009	0.806	12.5	5.8	4	foliation
84	pm17-7	423	875	2.16E-04	1.059	1.012	1.072	1.077	-0.643	-0.653	1.409	0.957	2.322	3	14.1	2.5	lineation
85	pm17-8	423	875	2.36E-04	1.034	1.018	1.053	1.054	-0.309	-0.320	0.985	0.984	1.726	3.6	6.9	2.4	lineation
86	pm17-9	423	875	2.42E-04	1.047	1.009	1.056	1.060	-0.671	-0.679	1.446	0.964	1.827	2.3	12.1	2	lineation
87	pm17-10	423	875	1.76E-04	1.025	1.006	1.032	1.034	-0.602	-0.607	1.344	0.981	1.043	5	19.6	4	lineation
88	pm18-1	423	875	1.40E-04	1.004	1.009	1.013	1.013	0.401	0.399	0.354	1.005	0.433	12.2	5.3	3.7	foliation
89	pm18-2b	423	875	1.36E-04	1.013	1.013	1.026	1.026	-0.004	-0.011	0.676	1.000	0.869	6.6	6.7	3.3	lineation
90	pm18-3b	423	875	1.39E-04	1.008	1.016	1.024	1.024	0.355	0.349	0.389	1.008	0.783	18.5	9.2	6.2	foliation
91	pm18-4	423	875	1.83E-04	1.013	1.003	1.016	1.017	-0.575	-0.577	1.302	0.991	0.536	7.4	25.9*	5.8	lineation
92	pm18-6	423	875	1.55E-04	1.020	1.009	1.029	1.030	-0.388	-0.394	1.070	0.989	0.961	13.9	29.6*	9.8	lineation
93	pm18-8	423	875	1.34E-04	1.007	1.018	1.024	1.025	0.459	0.455	0.316	1.011	0.796	14.3	5.5	4	foliation
94	pm18-9	423	875	2.58E-04	1.012	1.020	1.032	1.032	0.259	0.252	0.460	1.008	1.032	15.3	9.3	5.8	foliation
95	pm18-10	423	875	1.18E-04	1.010	1.024	1.034	1.035	0.410	0.403	0.351	1.014	1.125	15.9	6.9	4.9	foliation
96	pm19-1	423	875	2.72E-04	1.013	1.019	1.032	1.032	0.165	0.157	0.534	1.005	1.055	9.9	7.2	4.2	foliation
97	pm19-2	423	875	3.00E-04	1.040	1.012	1.053	1.055	-0.542	-0.551	1.267	0.973	1.723	5.1	17.2	4	lineation
98	pm19-4	423	875	2.29E-04	1.013	1.003	1.016	1.017	-0.677	-0.679	1.447	0.990	0.514	10.3	43.6*	8.7	lineation
99	pm19-5	423	875	1.89E-04	1.027	1.008	1.035	1.037	-0.527	-0.533	1.243	0.982	1.16	4.6	14.7	3.5	lineation
100	pm19-6	423	875	1.93E-04	1.009	1.019	1.028	1.029	0.373	0.367	0.376	1.010	0.919	11.3	5.3	3.6	foliation
101	pm19-7	423	875	1.82E-04	1.032	1.002	1.034	1.038	-0.877	-0.879	1.772	0.971	1.123	5.6	56.7*	5.3	lineation
102	pm19-8	423	875	2.34E-04	1.014	1.013	1.027	1.027	-0.067	-0.073	0.734	0.998	0.885	10.1	11.7	5.5	lineation
103	pm19-9	423	875	2.29E-04	1.029	1.009	1.039	1.040	-0.521	-0.528	1.237	0.981	1.263	5.2	16.4	4	lineation
104	pm19-10	423	875	2.35E-04	1.046	1.008	1.054	1.058	-0.716	-0.722	1.512	0.963	1.761	1.3	8.3	1.2	lineation
105	pm21-1	423	875	1.57E-04	1.012	1.017	1.029	1.029	0.163	0.156	0.535	1.005	0.942	19.3	14.4	8.4	foliation
106	pm21-2	423	875	1.68E-04	1.013	1.018	1.031	1.032	0.144	0.136	0.551	1.005	1.03	10.8	8.2	4.7	foliation
107	pm21-3	423	875	1.69E-04	1.018	1.019	1.037	1.037	0.041	0.032	0.639	1.002	1.22	3.6	3.4	1.7	foliation
108	pm21-4	423	875	1.90E-04	1.010	1.018	1.027	1.028	0.290	0.284	0.436	1.008	0.897	35.5*	21.7	14.3	foliation
109	pm21-6	423	875	2.68E-04	1.007	1.010	1.016	1.016	0.169	0.165	0.527	1.003	0.539	20.1	14.7	8.7	foliation
110	pm21-7	423	875	2.41E-04	1.007	1.006	1.013	1.013	-0.039	-0.042	0.705	1.000	0.431	15.8	17.1	8.4	lineation
111	pm21-8	423	875	2.40E-04	1.008	1.002	1.010	1.010	-0.593	-0.594	1.325	0.994	0.329	16.6	49.5*	13.3	lineation
112	pm21-9	423	875	2.30E-04	1.007	1.002	1.009	1.009	-0.665	-0.667	1.428	0.994	0.292	13.5	50.2*	11.3	lineation
113	pm21-10	423	875	1.69E-04	1.014	1.006	1.019	1.020	-0.417	-0.421	1.102	0.992	0.631	9.3	21.9	6.6	lineation
114	pm23-2b	423	875	2.37E-04	1.013	1.018	1.031	1.031	0.162	0.154	0.536	1.005	1.01	7.5	5.5	3.2	foliation
115	pm23-3	423	875	2.40E-04	1.025	1.010	1.035	1.036	-0.446	-0.452	1.140	0.985	1.156	5.9	15.3	4.3	lineation
116	pm23-8	423	875	2.57E-04	1.010	1.031	1.041	1.043	0.521	0.513	0.277	1.021	1.341	15.5	5.1	3.9	foliation
117	pm23-9	423	875	2.41E-04	1.014	1.003	1.017	1.018	-0.645	-0.647	1.400	0.989	0.56	9.3	37.4	7.7	lineation
118	pm23-10	423	875	2.27E-04	1.019	1.019	1.038	1.038	-0.012	-0.022	0.686	1.000	1.243	5.2	5.4	2.7	lineation
119	pm24-1	423	875	1.10E-04	1.052	1.003	1.055	1.062	-0.891	-0.894	1.798	0.953	1.802	4.7	55.5*	4.4	lineation
120	pm24-3	423	875	1.17E-04	1.013	1.020	1.033	1.033	0.221	0.213	0.490	1.007	1.071	9	5.9	3.6	foliation
121	pm24-4	423	875	1.39E-04	1.012	1.021	1.034	1.034	0.262	0.254	0.458	1.009	1.11	9.1	5.4	3.4	foliation
122	pm24-6	423	875	1.66E-04	1.011	1.016	1.027	1.028	0.178	0.172	0.522	1.005	0.9	6.8	4.8	2.8	foliation
123	pm24-8	423	875	2.84E-04	1.015	1.008	1.023	1.024	-0.287	-0.293	0.955	0.993	0.765	5.9	10.8	3.8	lineation
124	pm24-9	423	875	1.89E-04	1.009	1.012	1.021	1.021	0.172	0.167	0.526	1.004	0.696	10.1	7.3	4.3	foliation
125	pm24-10	423	875	1.51E-04	1.016	1.008	1.024	1.024	-0.301	-0.307	0.970	0.993	0.791	5.9	11	3.9	lineation
126	pm25-2	423	875	1.62E-04	1.013	1.005	1.018	1.019	-0.451	-0.455	1.143	0.992	0.605	9	22.9	6.6	lineation
127	pm25-3	423	875	2.21E-04	1.017	1.012	1.029	1.029	-0.157	-0.164	0.820	0.996	0.954	6.5	9	3.8	lineation
128	pm25-4	423	875	2.87E-04	1.011	1.025	1.037	1.038	0.376	0.368	0.375	1.014	1.205	8.8	4.1	2.8	foliation
129	pm25-7	423	875	2.16E-04	1.008	1.012	1.020	1.020	0.205	0.200	0.500	1.004	0.663	11	7.4	4.5	foliation
130	pm25-8	423	875	1.48E-04	1.008	1.004	1.013	1.013	-0.334	-0.337	1.004	0.996	0.421	30*	49.3*	21.1*	none
131	pm25-9	423	875	1.91E-04	1.014	1.007	1.021	1.021	-0.307	-0.312	0.976	0.994	0.69	8.7	16.2	5.7	lineation
132	pm25-10	423	875	1.76E-04	1.026	1.010	1.036	1.037	-0.425	-0.432	1.115	0.985	1.188	3.8	9.6	2.7	lineation

continued to next page

S. No.	Specimen	Field	Frequ-ency	Kmean (in SI)	L	F	P	P_J	T	U	Q	E	h%	e12	e23	e31	Dominant element
133	pm26-4	423	875	2.03E-04	1.012	1.003	1.015	1.016	-0.653	-0.655	1.412	0.991	0.481	4.9	22.4	4.1	lineation
134	pm26-5	423	875	1.33E-04	1.017	1.003	1.020	1.022	-0.674	-0.676	1.443	0.987	0.668	6.4	30	5.3	lineation
135	pm26-7	423	875	2.55E-04	1.029	1.010	1.039	1.041	-0.504	-0.511	1.214	0.981	1.283	3.5	10.7	2.7	lineation
136	pm26-8	423	875	1.60E-04	1.011	1.024	1.035	1.036	0.365	0.357	0.383	1.013	1.151	8.7	4.2	2.8	foliation
137	pm26-9	423	875	1.19E-04	1.037	1.006	1.043	1.046	-0.713	-0.718	1.505	0.971	1.401	3.6	20.8	3.1	lineation
138	pm26-10	423	875	2.28E-04	1.018	1.008	1.025	1.026	-0.398	-0.403	1.081	0.990	0.834	4.8	11.2	3.4	lineation
Tambarkurkur Formation																	
139	pt3-2c	423	875	1.14E-04	1.008	1.013	1.021	1.021	0.232	0.227	0.479	1.005	0.689	13.4	8.6	5.3	foliation
140	pt3-3b	423	875	2.07E-04	1.005	1.029	1.034	1.037	0.712	0.708	0.158	1.024	1.113	25	4.6	3.9	foliation
141	pt3-4b	423	875	1.81E-04	1.017	1.026	1.044	1.044	0.203	0.193	0.506	1.009	1.424	6.9	4.6	2.8	foliation
142	pt3-5	423	875	1.28E-04	1.013	1.008	1.021	1.022	-0.205	-0.211	0.868	0.996	0.703	7.7	11.7	4.7	lineation
143	pt3-6b	423	875	1.74E-04	1.024	1.055	1.080	1.082	0.380	0.363	0.379	1.030	2.558	6.3	2.9	2	foliation
144	pt3-7b	423	875	1.36E-04	1.018	1.004	1.022	1.024	-0.601	-0.605	1.340	0.987	0.737	10.7	37.5*	8.6	lineation
145	pt3-9b	423	875	2.07E-04	1.015	1.026	1.042	1.042	0.268	0.259	0.455	1.011	1.353	12.3	7.3	4.6	foliation
146	pt3-10b	423	875	1.43E-04	1.004	1.005	1.008	1.008	0.078	0.076	0.601	1.001	0.275	22.6	19.7	10.9	foliation
147	pt4-3b	423	875	1.56E-04	1.008	1.002	1.010	1.011	-0.679	-0.680	1.448	0.993	0.329	17.6	59*	14.9	lineation
148	pt4-4b	423	875	9.55E-05	1.002	1.009	1.011	1.012	0.581	0.579	0.235	1.007	0.371	62.6*	27.2*	22.1*	none
149	pt4-5b	423	875	1.07E-04	1.001	1.013	1.013	1.015	0.912	0.912	0.045	1.012	0.433	74.5*	9.5	9.1	foliation
150	pt4-6b	423	875	1.17E-04	1.003	1.011	1.014	1.015	0.519	0.516	0.275	1.007	0.473	36.2*	13.1	10	foliation
151	pt4-7b	423	875	6.67E-05	1.008	1.009	1.017	1.017	0.037	0.033	0.638	1.001	0.575	38.2*	36.4*	20.8*	none
152	pt4-7c	423	875	6.11E-05	1.009	1.012	1.021	1.021	0.135	0.129	0.556	1.003	0.692	38.2*	31.2*	18.9	none
153	pt4-8b	423	875	5.47E-05	1.041	1.004	1.045	1.050	-0.836	-0.840	1.703	0.964	1.476	4.9	44.6*	4.5	lineation
154	pt4-10b	423	875	5.73E-05	1.045	1.003	1.049	1.055	-0.856	-0.859	1.737	0.960	1.599	5.2	50.3*	4.9	lineation
155	pt4-11a	423	875	1.13E-04	1.013	1.003	1.015	1.016	-0.642	-0.644	1.395	0.990	0.507	9.1	36.6*	7.5	lineation
156	pt5-1b	423	875	1.32E-04	1.002	1.009	1.012	1.012	0.589	0.587	0.230	1.007	0.391	60.1*	24.3	19.7	foliation
157	pt5-3a	423	875	1.22E-04	1.008	1.009	1.017	1.017	0.077	0.072	0.604	1.001	0.562	38.6*	34.6*	20.3*	none
158	pt5-4b	423	875	5.94E-05	1.012	1.020	1.032	1.033	0.252	0.244	0.466	1.008	1.055	31.7*	20.6	13.2	foliation
159	pt5-5b	423	875	7.25E-05	1.007	1.012	1.019	1.019	0.235	0.231	0.476	1.004	0.627	24.1	15.7	9.8	foliation
160	pt5-7b	423	875	9.11E-05	1.004	1.004	1.009	1.009	-0.009	-0.011	0.676	1.000	0.285	31.5*	32.1*	17.2	none
161	pt5-8b	423	875	8.28E-05	1.019	1.007	1.027	1.028	-0.442	-0.447	1.134	0.988	0.88	7.3	18.6	5.3	lineation
162	pt5-10b	423	875	1.34E-04	1.013	1.025	1.039	1.039	0.303	0.294	0.429	1.012	1.257	9.1	5	3.2	foliation
163	pt12-2b	423	875	6.70E-05	1.001	1.001	1.002	1.002	0.001	0.000	0.667	1.000	0.067	59.5*	59.5*	40.4*	none
164	pt12-3	423	875	4.00E-05	1.037	1.017	1.054	1.055	-0.378	-0.390	1.065	0.980	1.759	5.8	13	4	lineation
165	pt12-4a	423	875	8.05E-05	1.003	1.010	1.013	1.014	0.554	0.552	0.252	1.007	0.433	39.6*	13.4	10.5	foliation
166	pt12-5	423	875	7.83E-05	1.002	1.003	1.004	1.004	0.302	0.301	0.424	1.001	0.14	67.4*	52.3*	40*	none
167	pt12-6	423	875	6.05E-05	1.005	1.010	1.015	1.015	0.359	0.356	0.384	1.005	0.479	40.4*	22	15.4	foliation
168	pt12-7	423	875	1.00E-04	1.004	1.011	1.015	1.016	0.514	0.512	0.278	1.008	0.496	33.1*	11.9	9	foliation
169	pt12-8	423	875	1.10E-04	1.002	1.010	1.012	1.013	0.641	0.640	0.198	1.008	0.387	38.7*	10	8.2	foliation
170	pt13-3	423	875	1.88E-04	1.005	1.012	1.017	1.017	0.440	0.437	0.328	1.007	0.545	22.7	9.3	6.7	foliation
171	pt13-4	423	875	2.41E-04	1.005	1.008	1.013	1.013	0.198	0.195	0.504	1.003	0.42	24.2	16.8	10.3	foliation
172	pt13-5	423	875	1.92E-04	1.011	1.004	1.016	1.016	-0.438	-0.441	1.126	0.993	0.52	8.1	20.2	5.9	lineation
173	pt13-6	423	875	2.04E-04	1.003	1.008	1.011	1.012	0.437	0.434	0.330	1.005	0.374	39.5*	18	13.1	foliation
174	pt13-7	423	875	2.16E-04	1.007	1.006	1.012	1.012	-0.072	-0.075	0.735	0.999	0.404	22.3	25.5*	12.4	lineation
175	pt13-2	423	875	2.06E-04	1.008	1.007	1.015	1.015	-0.076	-0.079	0.739	0.999	0.483	12.2	14.2	6.6	lineation
176	pt13-8	423	875	7.77E-05	1.002	1.005	1.007	1.007	0.299	0.298	0.426	1.002	0.232	57.5*	40.3*	28.8*	none
177	pt13-9	423	875	1.08E-04	1.005	1.004	1.009	1.009	-0.033	-0.035	0.698	1.000	0.305	29.6*	31.4*	16.4	none
178	pt13-10	423	875	1.71E-04	1.008	1.011	1.019	1.019	0.168	0.164	0.529	1.003	0.624	16.9	12.3	7.3	foliation
179	pt15-1	423	875	2.16E-04	1.020	1.005	1.024	1.026	-0.604	-0.608	1.345	0.986	0.805	7.2	27.5*	5.8	lineation
180	pt15-3b	423	875	2.02E-04	1.009	1.004	1.013	1.013	-0.426	-0.429	1.112	0.995	0.431	15.6	34.9*	11.3	lineation
181	pt15-3c	423	875	2.09E-04	1.013	1.011	1.024	1.024	-0.067	-0.073	0.733	0.998	0.787	9.2	10.6	4.9	lineation
182	pt15-6	423	875	1.90E-04	1.007	1.010	1.017	1.017	0.137	0.133	0.553	1.002	0.562	15.4	11.9	6.8	foliation
183	pt15-9	423	875	7.80E-05	1.006	1.003	1.008	1.009	-0.312	-0.313	0.978	0.997	0.279	23.9	40.3*	16.2	lineation
184	pt20-2	423	875	1.16E-04	1.004	1.004	1.008	1.008	0.071	0.069	0.607	1.001	0.266	22.5	19.9	10.9	foliation
185	pt20-3	423	875	5.73E-05	1.001	1.005	1.007	1.007	0.570	0.569	0.242	1.004	0.222	83.4*	67*	61.6*	none
186	pt20-7b	423	875	7.18E-05	1.012	1.004	1.016	1.017	-0.541	-0.543	1.257	0.992	0.527	12.7	37.3*	9.9	lineation
187	pt20-8	423	875	1.07E-04	1.018	1.006	1.024	1.025	-0.480	-0.485	1.181	0.989	0.799	10	27*	7.5	lineation
188	pt20-9	423	875	6.93E-05	1.006	1.002	1.008	1.008	-0.495	-0.496	1.195	0.996	0.256	20.3	47.7*	15.5	lineation
189	pt20-10	423	875	1.72E-04	1.010	1.005	1.015	1.015	-0.329	-0.332	0.999	0.995	0.48	7.4	14.6	5	lineation
190	pt22-3b	423	875	1.13E-04	1.015	1.008	1.022	1.023	-0.318	-0.323	0.988	0.993	0.736	16	29.2*	10.7	lineation
191	pt22-8	423	875	1.48E-04	1.009	1.006	1.015	1.015	-0.188	-0.191	0.848	0.997	0.51	18.7	26.5*	11.4	lineation

Nomenclature of AMS parameters L: magnetic lineation (kmax/kint, Balsley and Buddington 1960); F: magnetic foliation (kint/kmin, Stacey et al. 1960);
P: degree of anisotropy (kmax/kmin, Nagata 1961); E: foliation factor (kint^2/ kmax.kmin, Hrouda et al. 1971); q: anisotropy quantity (kmax-kint)/[(kmax+kint)/2-kmin], Granar 1958; Pj and T: Jelinek's corrected degree of anisotropy and shape parameter as defined in the text;
U: difference shape factor (2.kint-kmax-kmin)/(kmax-kmin), Jelinek 1981; h%: percent anisotropy (100*(kmax-kmin)/(kmax+kint+kmin), Tauxe et al. 1990.
Dominant elements (defined by thresholds of statistical parameters): lineation (e12 <= 25 deg); foliation (e23<= 25 deg); none (= isotropic) (e31>= 20)

Table 3: Site level mean AMS tensor elements

Site	Coordinates	n(N)	k_m (SI)	Max	Decl (°)	Incl (°)	Confidence ellipses (°) (a&b)		Int	Decl (°)	Incl (°)	Confidence ellipses (°) (a&b)		Min	Decl (°)	Incl (°)	Confidence ellipses (°) (a&b)	
Mukut Limestone																		
	In situ				225.8	10.3	9.0	4.3		355	74.1	14.1	6.5		133.6	12	12.8	4.6
pm01	Bed. cor. (BC)	7	**1.60E-04**	1.017	224.6	0.7			0.995	87.3	89.1			0.988	314.6	0.6		
	F plunge & BC				224.1	0.5	8.9	4.4		331.3	88.1	18.9	3.1		134.1	1.8	17.2	4.5
	In situ				231.7	13.3	19.1	10.2		339	51.3	51.7	9.7		132	35.6	52.0	7.1
pm02	Bed. cor. (BC)	8	**1.38E-04**	1.013	51.8	14.5			0.996	301	53.4			0.991	151.3	32.7		
	F plunge & BC				50.9	17.4	18.0	12.7		300.3	48.4	35.3	11.9		154.2	36.4	35.7	9.2
	In situ				59.8	52.9	32.1	11.4	1.024	152	1.6	30.5	4.5		243.2	37	17.7	7.1
pm06	Bed. cor. (BC)	8	**5.30E-04**	1.029	294.2	35.2	13.0	12.1		73.4	47	64.5	12.4	0.946	188.2	21.3	64.5	11.5
	F plunge & BC				298.6	18.4	26.6	20.2		200.0	24.2	54.9	19.1		62.0	58.9	55.1	17.7
	In situ				343.8	50.3	41.0	11.1		185	37.7	44.5	22.3		86.8	10.6	31.7	11.0
pm07	Bed. cor. (BC)	8	**1.72E-04**	1.005	2.2	57.3			1.000	175	32.6			0.996	267.2	3.2		
	F plunge & BC				2.5	57.0	41.0	11.0		175.0	32.8	44.7	22.2		267.2	3.4	32.0	10.9
	In situ				320.1	33.5	27.0	6.0		212	25.6	26.8	17		92.4	45.5	17.2	8.5
pm08	Bed. cor. (BC)	7	**1.36E-04**	1.012	338.0	21.6			1.002	205	60			0.986	76.2	19.9		
	F plunge & BC				338.9	18.1	29.3	9.4		213.6	60.5	28.9	15.1		76.7	22.5	19.6	7.6
	In situ				324.6	25.1	10.8	7.9		168	62.9	70.6	10.6		59.1	9.5	70.6	8.2
Pm09	Bed. cor. (BC)	9	**1.70E-04**	1.018	338.7	3.2			0.992	72.2	47.8			0.989	245.7	42		
	F plunge & BC				341.3	1.9	12.4	5.4		250.2	29.9	49.3	4.6		74.6	60.0	49.3	11.3
	In situ				16.8	33.4	28.5	14.7		172	54.1	29.0	17.7		278.9	11.8	19.3	14.5
Pm10	Bed. cor. (BC)	8	**1.64E-04**	1.010	12.4	3.9			1.001	182	86	29.0	17.7	0.989	282.3	0.8		
	F plunge & BC				191.7	1.4	23.5	12.6		92.1	81.6	24.3	17.9		281.9	8.3	19.2	12.5
	In situ				247.9	24.1	14.4	5.4		348	20.5	36.7	11.6		113.4	57.5	36.7	9.9
pm11	Bed. cor. (BC)	6	**2.06E-04**	1.017	67.0	11.1			0.995	331	29.6			0.988	175.3	58		
	F plunge & BC				66.8	11.1	14.9	6.1		330.1	30.9	31.0	10.9		174.2	56.8	30.6	10.5
	In situ				354.9	5.9	19.2	11.1		262	22.9	69.3	18.1		98.6	66.3	69.3	9.9
pm14	Bed. cor. (BC)	9	**1.64E-04**	1.012	174.0	10.7			0.995	274	42.1	69.3	18.1	0.993	72.7	45.9		
	F plunge & BC				175.2	11.2	17.9	11.1		269.2	19.1	68.7	16.8		56.4	67.6	68.7	9.3
	In situ				85.0	83.8	72.7	13.5		214	3.9	72.7	14		214.2	3.9	72.7	14.0
pm16	Bed. cor. (BC)	8	**2.26E-04**	1.007	30.6	63	72.7	13.5	1.004	216	26.9	72.7	10.9	0.989	125	2.2	16.1	10.9
	F plunge & BC				31.9	63.9	76.6	14.5		216.9	26.0	76.6	12.9		125.9	2.0	16.3	10.5
	In situ				45.9	13.0	19.5	8.8		297	54.4	57.1	18		144.4	32.5	57.1	10.5
pm17	Bed. cor.	9	**2.12E-04**	1.022	226.0	14.6			0.991	334	49.4	57.1	18	0.987	124.7	36.8		
	F plunge & BC				226.5	14.4	18.2	8.8		333.6	48.9	54.8	17.1		125.1	37.5	54.9	9.0
	In situ				51.9	21.1	38.5	16.4		167	47.8	38.1	9.1		306.5	34.5	18.9	8.5
pm18	Bed. cor. (BC)	8	**1.58E-04**	1.008	226.4	4.3			1.003	71.2	85.3	38.1	9.1	0.990	316.6	2		
	F plunge & BC				227.5	4.0	30.5	19.0		115.5	79.3	31.0	25.6		318.2	9.8	27.5	20.8
	In situ				2.6	42.4	10.8	8.8		212	15.4	34.2	8.2		107.2	15.4	34.3	9.6
pm19	Bed. cor. (BC)	9	**2.29E-04**	1.017	188.3	2.4			0.993	302	83.9	34.3	8.3	0.990	98.1	5.6		
	F plunge & BC				188.5	2.2	14.8	8.5		88.0	78.3	54.4	10.4		279.0	11.5	54.5	12.3
	In situ				354.7	13.7	15.1	9.9		184	76.1	15.4	8.1		85.2	2.2	12.2	6.7
pm21	Bed. cor. (BC)	9	**2.04E-04**	1.009	352.2	9.6			1.000	230	72.4	15.4	8.1	0.990	84.7	14.6		
	F plunge & BC				354.4	11.5	17.2	10.6		187.5	78.2	17.2	11.1		84.9	2.6	12.4	9.0
	In situ				16.0	56.7	7.2	3.0		136.7	5.1	10.2			236.4	26.6	9.6	2.8
pm23	Bed. cor.	5	**2.40E-04**	1.016	106.1	83.9			1.000	320	4.8		4.5	0.985	229.4	3.4		
	F plunge & BC				100.9	83.8	7.1	3.2		319.7	4.8	10.0	4.4		229.4	3.9	9.5	3.2
	In situ				37.3	22.3	20.6	14.0		143	34.1	30.4	20.3		280.8	47.4	30.3	14.2
pm24	Bed. cor. (BC)	6	**1.65E-04**	1.011	225.5	40.9			0.998	62.5	47.8	30.4	20.2	0.990	323	8.5		
	F plunge & BC				218.6	40.1	32.0	12.3		86.2	38.7	32.1	23.7		333.0	26.1	26.0	4.5
	In situ				252.7	0.3	40.2	21.4		161	54.4	44.9	25.2		342	35.6	36.7	22.1
pm25	Bed. cor. (BC)	7	**2.00E-04**	1.007	84.0	37.6			0.999	186	15	44.9	25.2	0.994	293.6	48.5		
	F plunge & BC				81.3	39.5	40.7	22.3		191.9	23.1	43.9	28.6		304.2	41.6	36.8	26.0
	In situ				202.1	10.4	16.6	11.5		47.8	78.5	18.6	12.4		293	4.9	21.7	9.5
pm26	Bed. cor. (BC)	6	**1.83E-04**	1.014	22.3	5.8			0.996	204	84.2		12.4	0.990	112.3	0.2		
	F plunge & BC				21.2	5.6	17.1	11.2		253.4	81.0	14.3	11.1		111.9	7.1	18.6	6.9

continued to the next page

Table 3 continued from the previous page

Site	Coordinates	n(N)	k_m (SI)	Max	Decl (°)	Incl (°)	Confidence ellipses (°) (a&b)		Int	Decl (°)	Incl (°)	Confidence ellipses (°) (a&b)		Min	Decl (°)	Incl (°)	Confidence ellipses (°) (a&b)	
Tambakurkur Formation																		
	In situ			1.012	97.7	37.9	36.7	4.4		338	32.7	36.3	5.7		220.9	35.1	9.1	5.3
pt03	Bed. cor. (BC)	8	**1.61E-04**		137.6	46.3			1.004	304	42.9			0.984	40.4	6.9		
	F plunge & BC				135.6	45.2	36.4	6.7		302.8	44.1	36.3	6.5		39.1	6.4	9.7	7.1
	In situ				28.5	60.2	10.1	4.8		275	13.1	10.4	9.4		177.9	26.2	10.1	5.1
pt04	Bed. cor. (BC)	9	**9.20E-05**	1.011	203.4	86.8			0.998	91.3	1.2			0.991	1.2	3		
	F plunge & BC				197.8	86.4	10.0	4.5		90.9	1.1	10.3	9.3		0.8	3.5	10.1	5.2
	In situ				251.3	75.2	60.9	12.6		29.4	11.1	60.9	14.9		121.3	0.7	17.9	8.6
pt05	Bed. cor. (BC)	7	**9.91E-05**	1.006	202.7	67.8			1.004	33.3	21.8			0.991	301.8	3.7		
	F plunge & BC				207.0	64.3	62.9	11.7		32.8	25.6	62.9	16.5		301.7	2.3	17.2	11.1
	In situ				222.3	39.0	39.1	15.3		2	43.3	38.9	16.6		113.8	21.5	22.0	5.6
pt12	Bed. cor. (BC)	7	**7.66E-05**	1.005	216.6	60.5			1.001	13.1	27.5			0.994	108.4	10.1		
	F plunge & BC				221.8	61.1	34.8	14.3		11.1	25.4	34.8	16.0		107.4	12.9	20.6	5.0
	In situ				333.5	58.3	69.6	12.4		182	28.6	69.7	13.8		84.7	12.6	21.6	8.3
pt13	Bed. cor. (BC)	9	**1.78E-04**	1.003	299.8	63.3			1.002	185	11.9			0.995	89.8	23.5		
	F plunge & BC				301.9	62.0	68.2	13.2		185.4	13.4	68.3	14.5		89.2	24.1	22.1	9.5
	In situ				306.2	0.1	11.7	3.2		36.2	14.8	23.2	10.1		215.9	75.2	22.9	3.2
pt15	Bed. cor. (BC)	5	**1.79E-04**	1.009	307.0	4.8			0.997	217	4.6	23.2	10.2	0.994	82.7	83.4		
	F plunge & BC				309.4	4.6	11.8	3.3		217.3	24.1	19.9	10.4		49.6	65.4	19.8	6.2
	In situ				27.2	30.7	18.1	9.7		127	14.8	16.9	10.7		238.9	55.2	16.4	8.2
pt20	Bed. cor. (BC)	5	**8.42E-05**	1.005	41.5	32.9			0.999	307	7.2			0.996	205.9	56.2		
	F plunge & BC				35.3	24.7	8.1	7.4		304.5	1.7	25.3	7.5		210.9	65.3	25.9	3.3
	In situ				335.7	30.4				244	2.3				150.4	59.5		
pt22	Bed. cor. (BC)	4	**1.37E-04**	1.009	349.8	18.7			0.996	247	33.5			0.995	104	50.3		
	F plunge & BC				353.0	19.3	23.7	2.5		261.1	5.3	82.3	19.8		156.4	69.9	82.3	2.6

Note: Max, Int and Min are the normalized principal AMS magnitudes. "F. plunge & BC" indicates a combined correction for plunge (126°/12°) and bedding tilt.

No significant differences by sampled lithofacies occur in the distribution of AMS axes among the geological units (MLF and TKF), though the former (pm sites) exhibit relatively higher susceptibilities (k_m) and anisotropy degree (PJ) than the latter (pt sites) (Fig. 5). To get an overview of the AMS directions, therefore, data on AMS axes for all sites are compared in situ, after correction for bedding-tilt and after 'effective bedding' correction (hereafter, used to denote a combined correction for the fold-plunge and bedding) (Fig. 6).

Visual examination of the AMS axes distributions with the plots of bedding planes and densities of k_{max} and k_{min} suggests a complex nature of the magnetic fabric comprising at least three patterns reflected more distinctly in the k_{max} axes. Specimens within the same site may exhibit mixed pattern owing to the presence of different types of AMS carriers (dia-, para- or ferro(i)magnetic minerals), variation in their relative concentrations and the varying degree of the development of alignments within the measured specimen volume (10 cc). AMS data at specimen level (Table 2) and site level (Table 3) can be used to understand the inter- and intra-site variations and also to compare them with (micro)structural observations, if any, and present the lineation and foliation data in the form of a map. Figure 7 shows the variation of mean magnetic lineation by sampled site in geographic and paleogeographic (after 'effective bedding' correction).

To reveal the major directional tendencies within the area, however, the specimen level data for anisotropic specimens (i.e., those with well-defined lineation and/or foliation) were examined through interactive plotting and grouping. The result is summarized as three distinct patterns of the distribution of principal AMS axes, which are described below and supplemented with stereonet plots and pattern-dependent summary parameters (Fig. 8, and lower part of Table 3).

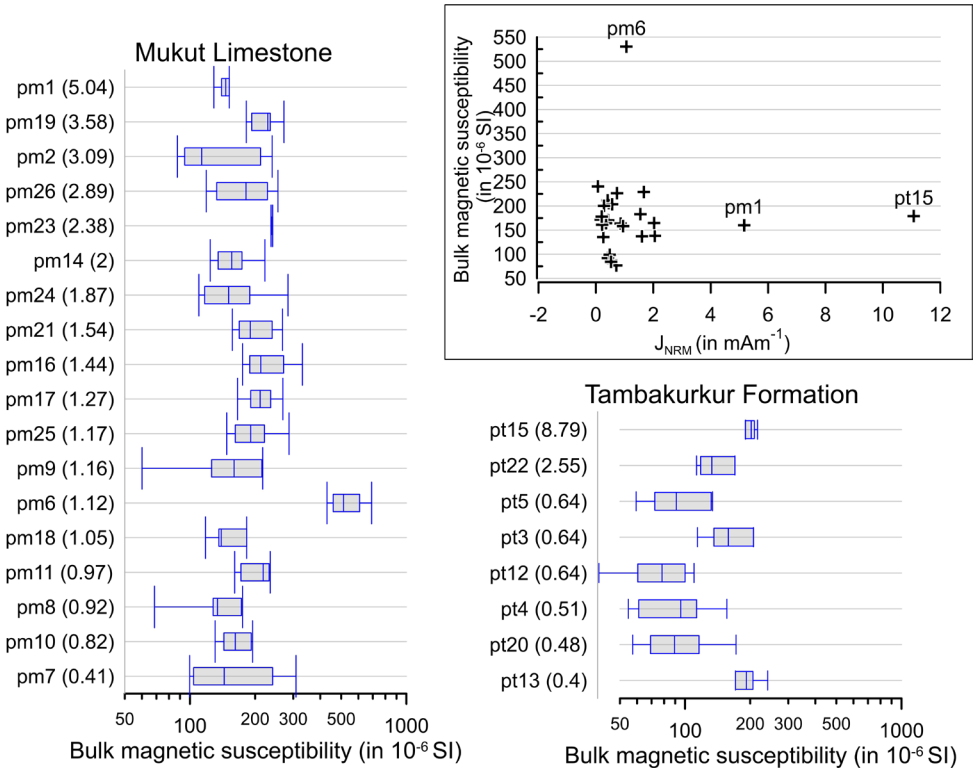

Fig. 4: Boxplots showing site-specific variation of magnetic susceptibility (minimum, 1st quartile, median, second quartile, maximum) of carbonates sampled from MLF (left) and Tambakurkur Formation (right). The inset is a biplot of magnitudes of susceptibility against the natural remanent magnetization intensity. For data, refer to Table 1.

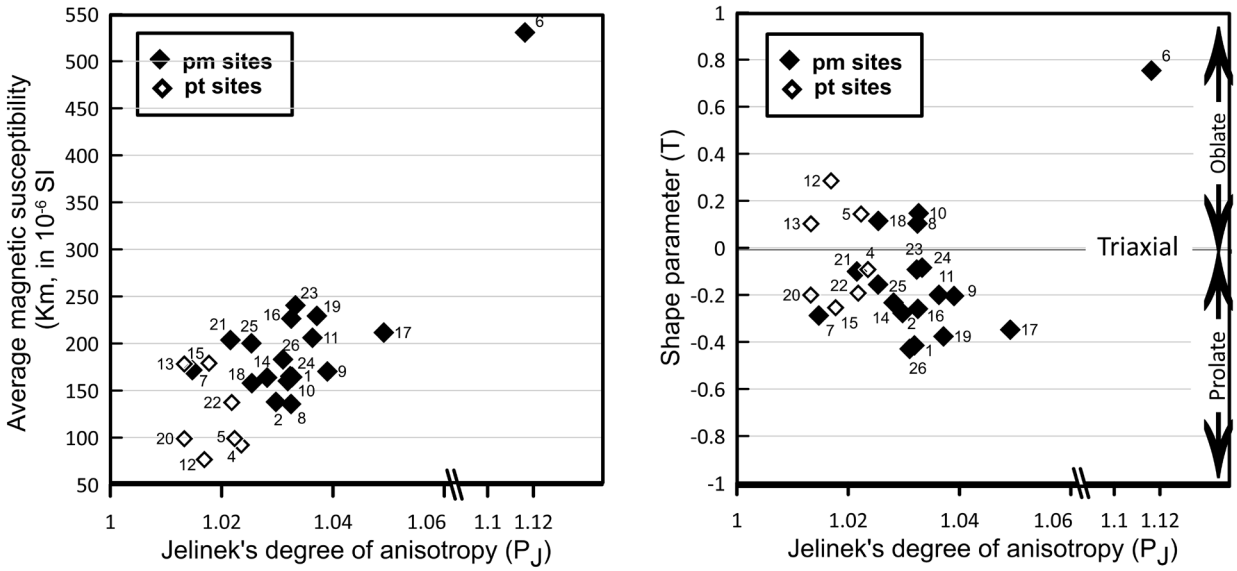

Fig. 5: Biplots (Km and T versus PJ) of selected scalar AMS parameters at the level of sampling site denoted by open and filled diamonds for the two formations (Tambakurkur and Mukut Limestone) to highlight the minor differences. Site pm6, located at the closure of a fold, exhibits extremely positive values in all parameters (high susceptibility, high anisotropy degree and highly oblate AMS ellipsoid).

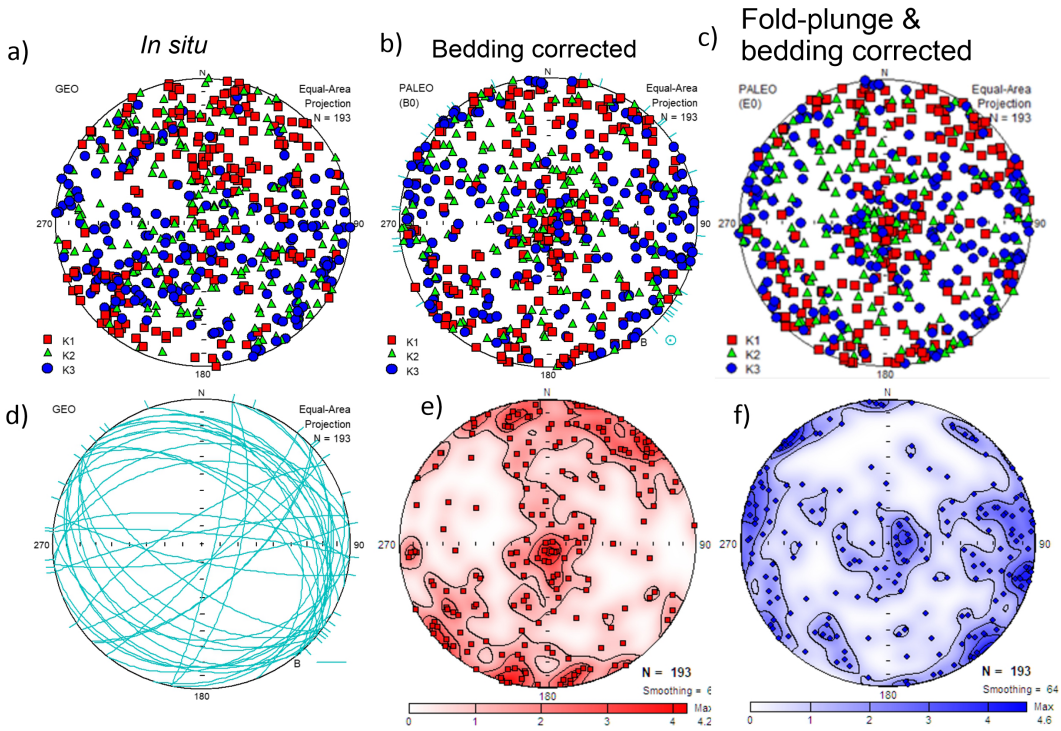

Fig. 6: a) Stereograms of principal AMS axes for 193 anisotropic specimens from all sites in geographic projection, b) bedding-tilt corrected, c) combined fold-plunge and bedding-tilt ('effective bedding') corrected coordinate systems, d) bedding strikes measured at sampled sites show their distribution mainly in shallow to moderate NE or SW dipping fold limbs, e) contour maps of the distribution of magnetic lineation (k_{max}), and f) magnetic foliation poles (k_{min}) both in bedding- tilt corrected system. These data reflect a composite magnetic fabric comprising at least two strong magnetic fabric patterns (MFPs) with k_{max} oriented NE-SW and N-S, in addition to a third minor pattern with sub-vertical k_{max}. These MFPs are resolved by an interactive visual analysis.

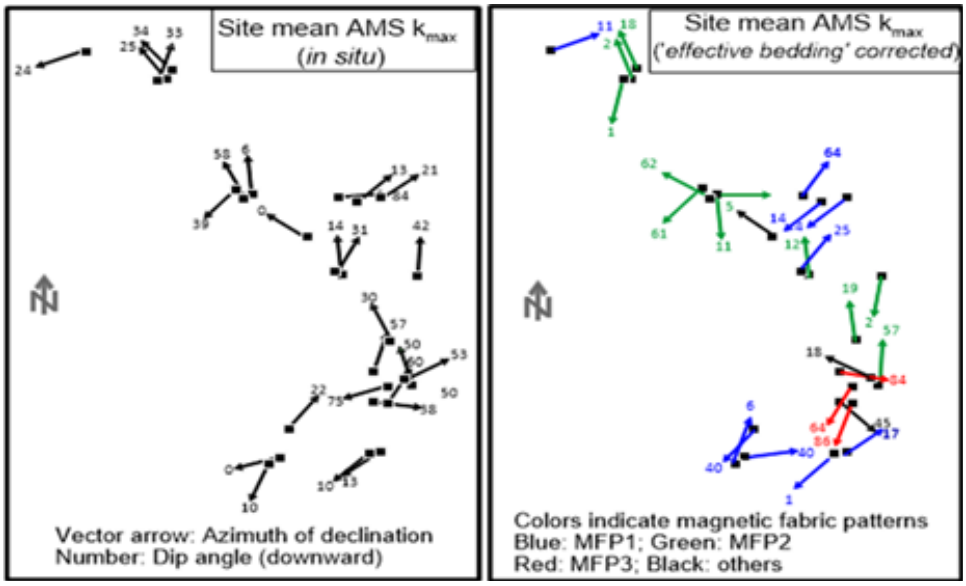

Fig. 7: Variation of mean k_{max} axes (magnetic lineations) in geographic and tectonic (fold-plunge and bedding corrected) coordinate systems using data compiled in Table 3. For the geological context of the sites (small squares), refer to Fig. 1. The remarkable scattering (a wide range of declinations and dips) of the site-mean k_{max} in geographic coordinates changes to at least three prominent groups (two shallow dipping groups pointing to either NE-SW (blue lines) or N-S directions (green lines), and a steeply dipping group (red lines)) after tectonic correction. These groups are identified as MFP1-3 patterns, of which the first two are important for understanding the structural development of the region.

Magnetic fabric pattern 1 (MFP1)

This group combines data for 69 specimens (from 10 sites) with specimen magnetic lineations (k_{max}) pointing mainly to NE or SW and dipping at shallow angles. Other two axes (k_{int} and k_{min}) are scattered along a NW- SE belt, with tendencies to concentrate towards the center and margins of the stereonet, respectively. MFP1 is observed at the SW part (sites pm1-2, pm24-26) of the study area and lens-shaped or isolated outcrops towards NE (sites pm16-19 and pt20). The majority of k_{min} axes are sub-horizontal being aligned parallel to the bedding strikes or the fold axes. Shallow to moderate dips for in situ k_{max} and k_{min} axes return to almost horizontal after bedding-tilt or effective tilt corrections, with slightly smaller confidence ellipses. The preferred peak estimates, obtained after 'effective bedding' correction, are as follows:

MFP1 magnetic lineation: Decl = *46.4°, Incl = 2.0°, Confidence ellipses (a, b): 31.6°, 21.8°*

MFP1 magnetic foliation pole: Decl = *316.4°, Incl = 1.2°, Confidence ellipses (a, b):43.1°, 21.8°*

Basic statistical calculations at the level of specimens (N=64) for MFP1 yield the following mean values: $k_m = 184.3 \pm 54.1 \times 10^{-6}$ SI; $P_J = 1.033 \pm 0.013$; $T = -0.227 \pm 0.399$. These values and the plots (Figs. 4 and 5) indicative of a low degree of anisotropy, and moderately prolate, triaxial and weakly oblate shapes are typical in sediments with paramagnetic minerals as dominant AMS carriers.

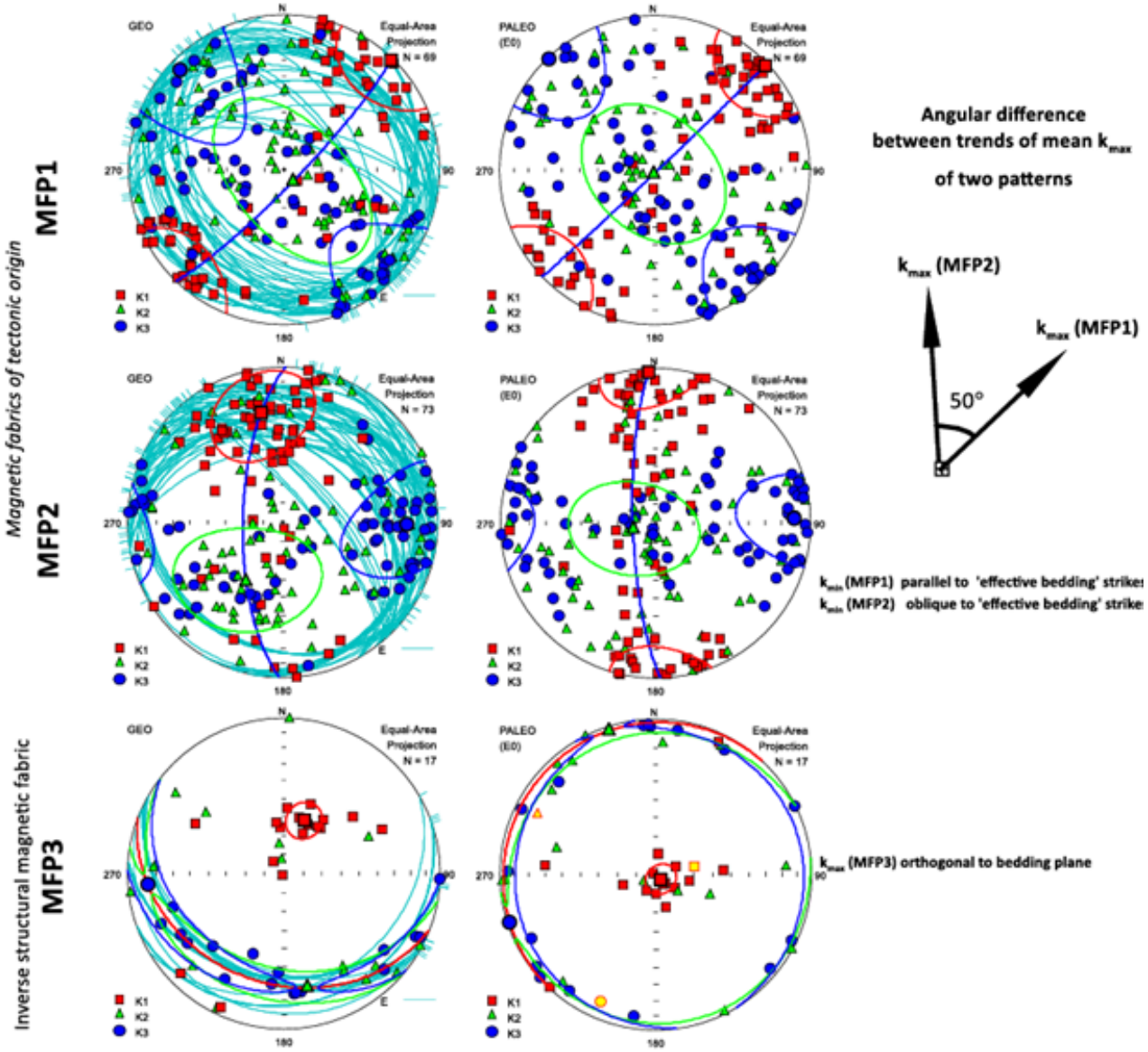

Fig. 8: Pairs of stereograms of principal AMS axes at the level of specimens from sites showing three distinct magnetic fabric patterns (MFP1-3) in geographic (left) and paleogeographic (right) coordinates. Light green great circles (E) represent 'equivalent bedding-tilt' attitudes obtained by joint correction for the plunge of the main fold (DMS) and beddings measured at the outcrop.

Magnetic fabric pattern 2 (MFP2)

This group combines data for 73 specimens (from 9 sites (pm7-10, pt12-13, pm14, pm21, pt22) with specimen magnetic lineations (k_{max}) pointing mainly towards north or south with a peak in situ Decl/Incl at 348.9°/29°. Both types of tilt corrections return k_{max} to almost horizontal position. The in situ k_{min} axes for most specimens lie along girdles in E-W sub-horizontal plane. After tilt correction, these axes show a strong tendency to align towards E or W margins. Estimates for means after 'effective bedding' correction are as follows:

MFP2 magnetic lineation: Decl=356.5°, Incl=2.6°, Confidence ellipses (a, b): 25.0°, 18.6°

MFP2 magnetic foliation pole: Decl=88.1°, Incl=11.8°, Confidence ellipses (a, b): 35.2°, 18.1°

For MFP2 (61 specimens), average scalar quantities are: k_m = 159.7±57.3×10^{-6} SI; P_J = 1.027±0.013, and T= - 0.050±0.396. Thus, MFP2 group is characterized by slightly lower average magnitudes of P_J and K_m and slightly more triaxial ellipsoid shapes compared to MFP1.

Magnetic fabric pattern (MFP3)

Magnetic lineations (k_{max}) are predominantly sub-vertical and these are orthogonal to the bedding planes which contain the other two axes. While the site pm23 representing MLF is a perfect example of such typical inverse magnetic fabric, a part of specimens in the two TKF sites (pt4 and pt5) exhibit different behavior. However, there is no objective way to exclude them. As k_{int} and k_{min} are intermingled along a great circle, the peak estimate is limited to the k_{max} suggestive of an inverse structural magnetic fabric. The best k_{max} estimate after 'effective bedding' correction is as follows:

MFP3 magnetic lineation: Decl=132.8°, Incl=86.5°, Confidence ellipses (a, b): 8.6°, 7.4°

Sites with isotropic or anomalous behavior inconsistent with MFP1-3 patterns

Three sites (pm6, pt3 and pt15) out of the total of 26 sites behaved differently than the others. For site pm6, situated at the closure of a fold and with specimens collected at spots with a range of bedding attitudes, the AMS axes are better grouped before any tilt correction (Table 3) with k_{max} axes close to the present-day geomagnetic field direction. This site was already described as anomalous also based on the elevated magnitudes of some scalar parameters (P, T, K_m) in the section Magnetic fabric charecteristics and illustrated in Figs. 4 and 5. Site pt3 specimens after 'effective bedding' correction exhibit NE-oriented horizontal k_{min} axes (like the k_{max} axes of MFP1) and a girdle along a NW-SE great circle that contains mutually separated linear arcs of k_{int} and k_{min} axes. Specimens from site pt15 exhibit yet another unique case, where the sub-horizontal k_{max} axes point to NW and the other two axes lie in separate arcs forming a girdle in NE-SW vertical plane after 'effective bedding' correction. The latter two sites may reflect local tectonic effects that are difficult to explain by existing observations. Thus, all three sites with features dependent on isolated sites, which are not representative of the prevailing AMS fabric patterns in the study area, will be ignored in further discussion.

INTERPRETATION AND DISCUSSION

The AMS-based magnetic fabric results from the crystallographic and shape preferred orientation (CPO and SPO) of all grains (ferro(i)magnetic, paramagnetic, and diamagnetic minerals) that grew, transformed and mobilized at different times, and also the mechanisms associated with depositional, diagenetic, and tectonic processes (Weil and Yonkee 2009). In the studied carbonates, preferential alignment of paramagnetic phyllosilicates (biotite, sericite and chlorite as the constituent metamorphic minerals) and ferro(i) magnetic minerals, i.e., magnetite including its maghemitized derivatives and pyrrhotite, which are evident from IRM data and AMS scalar parameters presented in the sections IRM analysis and Magnetic fabric charecteristics. Among the prominent magnetic patterns (MFP1-3), MFP1 and MFP2 differ in the orientations of all three principal AMS axes resulting in differences in the magnetic lineation (k_{max}) trends, orientation of magnetic foliation planes (great circles containing k_{max} and k_{int} or their poles corresponding to k_{min} axes), and the relationship between the magnetic foliation and the bedding planes (S0).

The MFP1 pattern with k_{min} axes (magnetic foliation poles) aligned approximately parallel to the fold axes and k_{max} forming NE-SW girdles resembles the AMS pattern P1 found in the Triassic carbonates in the Nar Phu valley, which is situated north of the Annapurna range in the Tethys Himalaya (Schill et al. 2003). Unlike a few sites with well-defined AMS fabric in Nar Phu, eight of the ten sites yielding MFP1 in Dolpo exhibit well-defined NE or SW oriented k_{max} axes, with shallow to moderate dips in geographic but sub-horizontal in paleogeographic coordinates (Table 2). These k_{max} axes are subparallel to the 'mineral stretching lineations' reported from non-carbonate lithologies occurring in areas adjacent to Dolpo: (i) the Mugu Karnali transect lying immediately to the West: generally NE-SW trending mineral and aggregate lineations with moderately NE and E-NE plunges within the LHS and GHC, respectively (Cannon and Murphy 2014); (ii) in situ mean mineral stretching lineations (trend/plunge) in STD (NW of Tinje: N56°E/34° and S48W/44°; SW of Dho: N76°E/25° (Cannon and Murphy 2014); and, (iii) biotite-based mineral lineations with ENE-WSW trend and SW plunge in the area situated South of the Mugu Granite as noted by Iaccarino et al. (2017). A sub-vertical NE-SW girdle formed by relatively better defined k_{max} axes alone or together with k_{int} axes represents a magnetic foliation resembling a 'cleavage' approximately orthogonal to the thrust front marked by the STD with its cartographic trace located ca. 20 km towards SW from the sampled area (Fig. 1b).

The MFP2 k_{max} axes exhibit northerly trends, which are 50° anticlockwise of the MFP1 k_{max} axes trends, in average (Table 3; Fig. 8). There is a similar difference between the peak sub-horizontal k_{min} declination estimates of the two patterns. Thus, while the dominantly NW or SE oriented MFP1 k_{min} axes generally coincide with the fold axes or the bedding strikes, a clearly oblique relationship is evident between the E or W oriented shallow dipping MFP2 k_{min} axes and the bedding strikes, fold axes or 'effective bedding' attitudes at the concerned sites (Fig. 8). In geographic coordinates, a reasonable parallelism exists between the MFP1 magnetic foliation poles (k_{min}) and fold axes/bedding strikes, but an

oblique relationship holds true between the MFP2 k_{min} and fold axes/bedding strikes. From a clear tendency of the AMS axes to cluster around mean estimates close to horizontal (for k_{max} and k_{min}) in paleogeographic coordinates favors the formation of the MFP1 more likely to have occurred prior to folding event accompanied by rotation and tilting. The significant angular difference (50°) between peak k_{max} of MFP1 and MFP2 may point to a succession of events by which the MFP1 developed earlier, followed by clockwise rotation of the area owing to tectonism, and MFP2 formed at a later stage.

A paleomagnetic study of all these sites (Crouzet et al. 2003) revealed a stable post-folding secondary characteristic remanences residing in pyrrhotite, whereas some 40% of them had preserved also a primary remanence of Triassic age carried by magnetite. Joint consideration of data on magnetic mineralogy (especially, pyrrhotite and magnetite as remanence carriers), the characteristic magnetic remanence types recovered and magnetic fabric patterns, suggests a strong affinity of MFP1 development to sites that yielded primary remanence carried by magnetite. Therefore, a genetic control of specific minerals on the fabric type (e.g., magnetite control on MFP1) is a possibility. From the primary nature of magnetite (a mineral of detrital origin and carrier of the primary remanence), but the secondary nature of pyrrhotite (an authigenic mineral formed by thermochemical processes during regional metamorphism partly at the expense of magnetite, and a carrier of secondary remanence), the MFP1 associated with sites that preserved magnetite was most likely formed earlier than the MFP2. Consequently, the MFP2 clearly reflects a later tectonic event giving rise to structures oblique to those represented by the MFP1.

The MFP3 pattern can be interpreted as inverse structural fabric (Černý et al. 2020), similar to that found in the marly/micaceous limestone from the TH and meta-carbonates from the MCT zone and the Mahabharat synclinorium in the midlands (Parsons et al. 2016; Gautam et al. 2025). Among the sites with this pattern, site pm23 clearly outstands by elevated k_m (227-241 $\times 10^{-6}$ SI) suggestive of the contribution of ferro(i) magnetic minerals, possibly the minor amounts of uniaxial/elongated single domain magnetite (UDM) known to exhibit a reverse fabric (Rochette 1988; Tauxe 2002). Černý et al. (2020), in a review of numerous AMS case studies, described an inverse magnetic fabric related to a cone-in-cone structure developed in low-competent material (shale and siltstone) with cone apexes directed towards the competent beds bounding it. The siltstones contained fibrous crystals of paramagnetic iron-bearing carbonate (ankerite and siderite) with PCO parallel to the cone-in-cone microstructural axis (also parallel to the k_{max}). In that case, the long axes of the iron-bearing carbonates tended to be perpendicular to the bedding plane. In our carbonates that are poor in ferro(i)magnetic minerals, one of the possible causes for the observed inverse anisotropy is the preferential growth of the paramagnetic iron-containing minerals (formed by replacing Ca in calcite and dolomite) along vertical (orthogonal to the bedding) microstructures. One plausible case would be the presence of stylolites (with a wavelength of a few mm and formed within the carbonate succession affected by shortening in the direction perpendicular to the bedding plane. Possibility of the parallelism between compression and the long axis of the magnetite grains (or clusters of isometric grains) due to mimicking of the shape of the stylolitic peaks was pointed also by Rochette (1988). Such an inference, however, needs to be verified through further investigations into the AMS carrying minerals and the microstructures accommodating the preferential growths of such carriers using an integrated optical, crystallographic preferred orientation (CPO), and image analyses (e.g., Nania et al. 2024).

This study revealed three distinct fabric patterns, of which the first two (MFP1and2) offer potential for understanding the tectonics of the Himalayan orogen (e.g., temporal changes in the direction of India-Eurasia convergence, amounts of rotations due to possible oroclinal bending and block rotations, etc. as pointed by Appel et al. 1991). The newly acquired magnetic fabric data should aid better interpretation by integrating these data with further direct observations on microstructures either in the field or laboratory on the carbonates from an area broader than that covered by this study and also additional structural and/or magnetic fabric measurements on more heterogenous facies other than carbonates in adjoining areas.

CONCLUSIONS

Our exploratory AMS study of the low metamorphic grade carbonates from Dolpo reveals two major fabric patterns characterized by magnetic lineations (k_{max} axes) with contrasting trends along NE-SW and N-S directions, respectively. Their mean lineations turn to be sub-horizontal with significant angular difference of 50° while the magnetic foliation poles (k_{min} axes) also turn to NW-SE and E-W sub-horizontal positions after combined correction for the gentle plunge of the major fold and bedding attitudes. Concerning the first pattern, a sub-parallelism of the observed magnetic lineations with regional stretching lineations (recorded by rocks in geotectonic units subjected to higher metamorphic grades and occurring at some distance from the study area,), the sub-vertical nature of the magnetic foliations, and parallelism between the magnetic foliation poles and fold axes/bedding strikes support a tectonic origin. An affinity of the sites yielding the first pattern (MFP1) with those known to possess magnetite-based primary remanence suggests the possible role of magnetite also as an AMS carrier. whereas the second pattern (MFP2) seems to be controlled by processes leading to the production of pyrrhotite, which is ubiquitous in the area as a secondary remanence carrier but may not directly contribute to the AMS fabric. The magnetic lineations characterizing MFP2 may be better considered as the reflections of India-Eurasia compressive regime during the late Tertiary times. AMS fabric data on the linear and planar fabric elements seen in the two contrasting patterns complement the multidisciplinary data from the Tethys Himalaya for use in elaboration of the tectonic development of the Higher Himalayan region.

A third minor magnetic fabric pattern with the k_{max} axes

orthogonal to bedding (S0) that is subparallel to the girdle defined by the other two axes (k_{int} and k_{min}) represents an inverse structural magnetic fabric most likely carried out by uniaxial/elongated single domain magnetite. This inverse fabric is of theoretical interest.

ACKNOWLEDGEMENT

This study was initiated as a part of project AP34/9(1-3) (PI: E. Appel) funded by the German Research Foundation (DFG). The field work in Nepal involved collaboration between University of Tuebingen (Germany) and Tribhuvan University (Nepal) to which the first author was affiliated in the past.

REFERENCES

Appel, E., Schill, E., and Crouzet, C., 2012, Pyrrhotite remagnetizations in the Himalaya: a review. Geological Society, London, Special Publications, v. 371(1), pp. 163, https://doi.org/10.1144/sp371.1

Appel, E., Müller, R., and Widder, R.W., 1991, Palaeomagnetic results from the Tibetan Sedimentary Series of the Manang area. north central Nepal, Geophysical Journal International, v. 104 (2), pp. 255–266.

Balsley, J.R., and Buddington, A.F., 1960, Magnetic susceptibility anisotropy and fabric of some Adirondack granites and orthogneisses. American Journal of Science, v. 258A, pp. 6–20.

Cannon, J.M., and Murphy, M.A., 2014, Active lower crustal deformation and Himalayan seismic hazard revealed by stream channels and regional geology. Tectonophysics, v. 633, pp. 34–42. https://doi.org/10.1016/j.tecto.2014.06.031

Carosi, R., Montomoli, C., and Visona, D., 2007, A structural transect in the lower Dolpo: insights on the tectonic evolution of Western Nepal. Journal of Asian Earth Sciences, v. 29, pp. 407–423. https://doi.org/10.1016/j.jseaes.2006.05.001

Černý, J., Melichar, R., Všianský, D. and Drahokoupil, J., 2020, Magnetic anisotropy of rocks: A new classification of inverse magnetic fabrics to help geological interpretations. Journal of Geophysical Research: Solid Earth, v. 125, pp. e2020JB020426. https://doi.org/10.1029/2020JB020426

Chadima, M., 2018, Anisoft - Advanced treatment of magnetic anisotropy data.EGU General Assembly Conference Abstracts, 15017.

Colchen, M., Le Fort, P., and Pêcher, A., 1981, Geological map of Annapurnas-Manaslu-Ganesh Himalaya of Nepal, In: Gupta, H.K., and Delany, F.M. (eds.), *Zagros-Hindu Kush-Himalaya geodynamic evolution*. American Geophysical Union, scale 1:200,000.

Coleman, M.E., 1996, Orogen-parallel and orogen-perpendicular extension in the central Nepalese Himalayas. Geological Society of America Bulletin, v. 108, pp. 1594–1607.

Crouzet, C., Dunkl, I., Paudel, L., Arkai, P., Rainer, T.M., Balogh, K., and Appel, E., 2007, Temperature and age constraints on the metamorphism of Tethyan Himalaya in Central Nepal: a multidisciplinary approach. Journal of Asian Earth Sciences, v. 30, pp. 113–130.

Crouzet, C., Gautam, P., Schill, E., and Appel, E., 2003, Multicomponent magnetization in western Dolpo (Tethyan Himalaya, Nepal): tectonic implications. Tectonophysics, v. 377 (1-2), pp. 179-196.

Dearing, J., 1999, Magnetic susceptibility. In: Walden J, Oldfield F, and Smith J (eds.), *Environmental Magnetism: A Practical Guide*, pp. 35–62.

Dhital, M.R., 2015, *Geology of the Nepal Himalaya: Regional Perspective of the Classic Collided Orogen.* Springer.

Dunlop, D.J., and Özdemir, Ö., 1997, Rock Magnetism. Fundamentals and Frontiers, Cambridge Studies in Magnetism Series. Cambridge University Press, v. xxi, pp. 573,

Fuchs, G., 1973, On the Geology of the Karnali and Dolpo Regions, West Nepal. Austrian Journal of Earth Sciences, v. 66-67, pp. 21-32.

Fuchs, G., 1977a, Geological map of western Dolpo, Nepal (scale 1:80000). Jahrbuch der Geologischen Bundesanstalt, v. 120, pp. 15.

Fuchs, G., 1977b, The geology of the Karnali and Dolpo regions, western Nepal. Jahrb, Geol. Bundesanst, v. 120, pp. 165-217.

Garzanti, E., 1999, Stratigraphy and sedimentary history of the Nepal Tethys Himalaya passive margin. Journal of Asian Earth Sciences, v. 17, pp. 805-827.

Garzanti, E., Gorza, M., Martellini, L., and Nicora, A., 1994, Transition from diagenesis to metamorphism in the Paleozoic to Mesozoic succession of the Dolpo Manang synclinorium and Thakkola Graben (Nepal Tethys Himalaya). Eclogae Geologicae Helvetiae, v. 87, pp. 613–632.

Garzione, C.N., Dettman, D.L, Quade, J., DeCelles, P.G., and Butler, R.F., 2000, High times on the Tibetan Plateau: Paleoelevation of the Thakkhola graben, Nepal. v. Geology 28(4), pp. 339–342. doi: https://doi.org/10.1130/0091-7613(2000)28<339:HTOTTP>2.0.CO;2

Gautam, P., Regmi, K.R., and Appel, E., 2025, Inverse magnetic fabric in the carbonates from the Mahabharat Synclinorium, Lesser Himalaya, Nepal. *Manuscript submitted to the Bulletin of the Department of Geology, Tribhuvan University.*

Gautam, P., Yoshida, K., Dhital, M.R., Suzuki, S., Kawamura, T., and Gyawali, B.R., 2024, Superposed remanent magnetization and magnetic fabric in Triassic carbonates of Tethys Himalaya (Jomsom area, Nepal): chronological and tectonic implications. Journal of Nepal Geological Society, v. 67(1), pp. 107–126. https://doi.org/10.3126/jngs.v67i1.74590

Godin, L., 2003, Structural evolution of the Tethyan sedimentary sequence in the Annapurna area, central Nepal Himalaya, Journal of Asian Earth Sciences, v. 22, pp. 307–328.

Glesson, T.P., and Godin, L. 2006, The Chako antiform: A folded segment of the Greater Himalayan sequence, Nar valley, Central Nepal Himalaya. Journal of Asian Earth Sciences, v. 27, pp. 717–734.

Godin, L., Gleeson, T., Searle, M.P., Ullrich, T.D., and Parrish, R.R., 2006, Locking of southward extrusion in favor of rapid crustal-scale buckling of the Greater Himalayan sequence, Nar valley, central Nepal, In: Law, R.D. Law, Searle, M.P., and Godin, L. (eds.), *Channel Flow, Ductile Extrusion, and Exhumation in Continental Collision Zones.* Geological Society, London, Special Publication, v. 268, pp. 269-292.

Granar, L., 1958, Magnetic measurements on Swedish varved sediments. Arkiv. f. Geofysik, v. 3, pp. 1–40.

Hrouda, F., 2004, Problems in interpreting AMS parameters in diamagnetic rocks. Geological Society, London, Special Publications, v. 238(1), pp. 49–59. https://doi.org/10.1144/GSL.SP.2004.238.01.05

Hrouda, F., Janak, F., Rejl, L., and Weiss, J., 1971, The use of magnetic susceptibility anisotropy for estimating the ferromagnetic mineral fabrics of metamorphic rocks. Geologische Rundschau v. 60, pp. 1124–1142.

Hunt, C., Moskowitz, B.M., and Banerjee, S.K., 1995, Magnetic properties of rocks and minerals. In: Ahrens T.J. (Ed.), *Handbook of Physical Constants*, American Geophysical Union, v. 3, pp. 189-204.

Hurtado, J., Chatterjee, N., Ramezani, J., Hodges, K., and Bowring, S., 2007, Electron Microprobe Chemical Dating of Uraninite as a Reconnaissance Tool for Leucogranite Geochronology. Available from: https://www.nature.com/articles/npre.2007.655.1

Iaccarino, S., Montomoli, C., Carosi, R., Massonne, H.-J., and Visonà, D., 2017, Geology and tectono-metamorphic evolution of the Himalayan metamorphic core: insights from the Mugu Karnali transect, Western Nepal (Central Himalaya). Journal of Metamorphic Geology, v. 35, pp. 301–325. https://doi.org/10.1111/jmg.12233

Jelinek, V., 1981, Characterization of the magnetic fabric of rocks. Tectonophysics v. 79, pp. T63-67.

Kruiver, P.P., Dekkers, M.J., and Heslop, D., 2001, Quantification of magnetic coercivity components by the analysis of acquisition curves of isothermal remanent magnetization. Earth and Planetary Science Letters, v. 189, pp. 269–276.

Lascu, I., Banerjee, S.K., and Berquó, T.S., 2010, Quantifying the concentration of ferrimagnetic particles in sediments using rock magnetic methods. Geochemistry, Geophysics, Geosystems, v. 11, pp. Q08Z19, https://doi.org/10.1029/2010GC003182

Le Fort P., 1986, Metamorphism and magmatism during the Himalayan collision. In: Coward, M.P., and Ries, A.C. (eds.), Collision tectonics, Geological Society special publication, v. 19, pp. 159-172.

Nagata, T., 1961, Rock Magnetism, Maruzen, Tokyo.

Nania, L., Montomoli, C., Iaccarino, S., and Carosi, R., 2024, Calcite fabric development in calc-mylonite during progressive shallowing of a shear zone: An example from the South Tibetan Detachment system (Kali Gandaki valley, Central Himalaya). Tectonophysics, v. 872, pp. 230176. https://doi.org/10.1016/j.tecto.2023.230176

Parsons, A.J., Ferré, E.C., Law, R.D., Lloyd, G.E., Phillips, R.J., and Searle, M.P., 2016, Orogen-parallel deformation of the Himalayan midcrust: Insights from structural and magnetic fabric analyses of the Greater Himalayan Sequence, Annapurna-Dhaulagiri Himalaya, central Nepal. Tectonics v. 35, pp. 2515–2537, https://doi.org/10.1002/2016TC004244

Peters, C., and Dekkers, M.J., 2003, Selected room temperature magnetic parameters as a function of mineralogy, concentration and grain size. Physics and Chemistry of the Earth, Parts A/B/C, v. 28 (16–19), pp. 659-667.

Petrovský, E., and Kapička, A., 2006, On determination of the Curie point from thermomagnetic curves. Journal of Geophysical Research 111, B12S27, http://dx.doi.org/10.1029/2006JB004507

Roberts, A.P., Florindo F., Chang L., Heslop D., Jovane L., and Larrasoaña, J.C., 2013, Magnetic properties of pelagic marine carbonates. Earth-Science Reviews, v. 127, pp. 111-139, https://doi.org/10.1016/j.earscirev.2013.09.009

Rochette, P., 1987, Magnetic susceptibility of the rock matrix related to magnetic fabric studies. Journal of Structural Geology, v. 9(8), pp. 1015-1020, https://doi.org/10.1016/0191-8141(87)90009-5

Rochette, P., 1988, Inverse magnetic fabric in carbonate-bearing rocks. Earth and Planetary Science Letters, v. 90, pp. 229–237, https://doi.org/10.1016/0012-821X(88)90103-3

Rochette, P., Scaillet, B., Guillot, S., LeFort, P., Pecher, A., 1994, Magnetic properties of the High Himalayan leucogranites: structural implications. Earth and Planetary Science Letters, v. 126, pp. 214-234.

Schill, E., Appel, E., Godin, L., Crouzet, C., Gautam, P., and Regmi, K.R., 2003, Record of deformation by secondary magnetic remanences and magnetic anisotropy in the Nar/Phu valley (central Himalaya). Tectonophysics, v. 377, pp. 197–209.

Schneider, C., and Masch, L. 1993, The metamorphism of the Tibetan Series from the Manang area, Marsyandi valley, central Nepal. In: Treloar, P.J., and Searle, M.P. (eds.), *Himalayan Tectonics*. Geological Society, London, Special Publications, v. 74, pp. 357–374.

Searle, M.P., and Godin, L. 2003, The South Tibetan detachment system and the Manaslu leucogranite: a structural reinterpretation and restoration of the Annapurna – Manaslu Himalaya, Nepal. Journal of Geology, v. 111, pp. 505–524.

Stacey, F.D., Joplin, G., and Lindsay, J., 1960, Magnetic anisotropy and fabric of some foliated rocks from S.E. Australia. Geofisica Pura et Applicata, v. 47, pp. 30–40.

Stutz, James K., 2012, Geometry of the Dolpo-Mugu folds: Implications for the deep crustal structure of central Nepal. M. Sc. Thesis, Department of earth and atmospheric science, University of Houston, 2012.

Tauxe, L., Constable, C., Stokking, L., and Badgley, C., 1990, Use of anisotropy to determine the origin of characteristic remanence in the Siwalik red beds of northern Pakistan. Journal of Geophysical Research: Solid Earth v. 95(B4), pp. 4391-4404, DOI: 10.1029/JB095iB04p04391

Tauxe, L., 2002, Paleomagnetic Principles and Practice. Springer, Dordrecht, pp. 311,

Weil, A.B., and Yonkee, A., 2009, Anisotropy of magnetic susceptibility in weakly deformed red beds from the Wyoming salient, Sevier thrust belt: Relations to layer-parallel shortening and orogenic curvature. Lithosphere, v. 1(4), pp. 235–256, https://doi.org/10.1130/L42.1

Zhang Q., Appel E., Stanjek H., Byrne J.M., Berthold C., Sorwat J., Rösler W., and Seemann T., 2020, Humidity related magnetite alteration in an experimental setup. Geophysical Journal International, v. 224(1), pp. 69–85, https://doi.org/10.1093/gji/ggaa394.